Journal of the Brazilian Society of Mechanical Sciences and Engineering (2018) 40:303
https://doi.org/10.1007/s40430-018-1225-2

REVIEW

Nanofluids for heat transfer applications: a review

Tiago Augusto Moreira[1] · Debora Carneiro Moreira[1] · Gherhardt Ribatski[1]

Received: 17 December 2017 / Accepted: 11 May 2018 / Published online: 22 May 2018

Abstract

Since diluted suspensions of nanoparticles were first called nanofluids and presented as viable solutions for heat transfer applications, this subject has received much attention and related investigations have expanded to many paths. In order to comprehend how nanoscale-related effects could influence the macroscopic transport behavior of nanofluids under single or phase-change conditions, researchers have studied, for example, the stability of these solutions, variation of thermal and rheological properties, and the convective heat transfer behavior of a great variety of nanofillers in common fluids, mainly water. The deposition of nanofillers over heated surfaces has also been investigated due to the role of surface nanostructuring in modifying wettability, thermal resistance, and delaying the occurrence of critical heat flux. Despite the considerable number of publications regarding nanofluids, scattered results for transport properties or convective behavior of nanofluids under similar experimental conditions are often found, which hinders their applications due to a lack of comprehension on the mechanisms related to the behavior of these fluids and, consequently, to the difficulty in predicting it. In this context, this work concerns a review about the heat transfer behavior of nanofluids under single-phase flow, pool boiling, and flow boiling conditions. In general, there is a consensus that the heat transfer coefficient of single-phase flow is enhanced by the addition of nanoparticles to base fluids, although overall benefits of their application cannot be assured due to increases in viscosity. In contrast, either increase or decrease in heat transfer coefficient could be observed for pool and flow boiling conditions. Such behavior can be attributed to surface modifications due to interactions between the bare surface texture and the deposited nanoparticles; however, information on the surface texture is commonly missing in most works. Finally, the main mechanisms reported in the literature pointed out as responsible for the heat transfer coefficient behaviors are summarized, where it can be seen that modifications of transport properties and particles movements impact single-phase flow, while phase-change heat transfer is also influenced by variations of surface characteristics.

Keywords Nanofluid · Convection · Boiling · Transport properties · Phase change

List of symbols

c_p	Specific heat [J/(kg K)]
d	Channel diameter (m)
d_p	Particle diameter (m)
g	Gravity acceleration (m/s^2)
G	Mass velocity [kg/(m^2 s)]
h	Heat transfer coefficient [W/(m^2 K)]
k	Thermal conductivity [W/(m K)]
n	Configuration factor
p	Pressure (kPa)
q	Heat flux (kW/m^2)
r_c	Critical radius (m)
r_{np}	Particle radius (m)
R_{bd}	Interfacial thermal resistance (K/W)
T	Temperature (°C)
v	Sedimentation velocity (m/s)
V	Flow velocity (m/s)
x	Vapor quality

Greek symbols

α	Thermal conductivity ratio
ϕ	Particles volume fraction
ϕ_m	Particles mass fraction
λ	Minimum spacing between particles (m)
ρ	Density (kg/m^3)
σ	Surface tension (N/m)
ψ	Sphericity

Technical Editor: Francis HR Franca.

✉ Debora Carneiro Moreira
dcmoreira@usp.br

[1] Heat Transfer Research Group, São Carlos School of Engineering, University of São Paulo, São Carlos, SP, Brazil

Subscripts

bf Base fluid
in Inlet
nf Nanofluid
np Nanoparticle

Abbreviations

CHF Critical heat flux
HTC Heat transfer coefficient
PVA Polyvinyl acetate

1 Introduction

The ability to dissipate or absorb heat in restricted spaces is a major challenge for the development of electronic devices and concentrated solar energy converters. In this way, during the last decades, much effort has been employed in order to attend the increasing demands for heat absorption and spreading in such equipments [1]. Researchers indicate that the substitution of traditional air cooling systems by liquid cooling ones is a promising solution to satisfy the increasing demand for high heat flux removal, maintaining low temperature gradients and wall overheating [2]. Among the available cooling methods, single- or multiple-phase flows through microchannels have been extensively investigated and presented favorable results [3, 4], especially when associated with heat recovering systems [5, 6]. However, there is much to be improved in order to achieve the full potential of these most promising cooling methods [7]. In this context, modifying the transport properties of fluids to intensify the heat transfer coefficient (HTC), for example, has been indicated as a possible method to improve the performance of heat spreading systems. Choi and Eastman [8] suggested that diluted suspensions of metallic nanoparticles, which they called nanofluids, could be employed as improved refrigerants in heat exchanging systems, and also investigated the feasibility of using such fluids.

Inspired by Choi and Eastman's work [8], many investigations regarding nanofluids were carried out. Researchers have investigated, for example, various methods to produce stable nanofluids [9], the influence of nanoparticles addition in distinct base fluid physical properties, and single- or two-phase heat transfer behavior of nanofluids [10]. For instance, Yang et al. [11] measured the convective HTC of single-phase laminar flows of graphite-loaded nanofluids in a horizontal tube. In their study, they found thermal conductivity enhancements of up to 56%, which improved the heat transfer coefficient. Nevertheless, the use of nanofluids also implies on increment in the pumping power for a fixed mass flow rate due to higher pressure drops, if compared with pure base fluids flows. This rise in pumping power is directly related to an increment in the base fluids' viscosity caused by the addition of nanoparticles [12].

Majority of investigations regarding nanofluids are focused on thermophysical properties of the fluids and heat transfer behavior under single-phase flow, as can be verified in some literature reviews [13, 14]. Phase-change heat transfer, however, has also been investigated, and numerous works that deal with pool boiling of nanofluids can be found [15], while fewer studies regarding flow boiling of nanofluids have been carried out [16]. Despite the substantial number of publications in this field, distinct research groups often report scattered results for similar experimental conditions, which corroborate the need for additional investigations focusing on the physical mechanisms responsible for the observed behaviors [17, 18]. In this context, a broad literature review was conducted in the present work, in order to reveal the state of the art of nanofluids and critically analyze previous experimental results together with their interpretation. In this way, the historical evolution of nanofluid investigations is presented, and some methods for preparation, stabilization, and characterization of nanofluids are described, and then, the results are discussed. Finally, studies involving single-phase and boiling heat transfer behavior of nanofluids are reviewed, and the main conclusions found in the literature regarding heat transfer mechanisms are summarized.

2 Historical perspective

Masuda et al. [12] conducted a pioneering study where they proposed and evaluated the influence of nanoparticles insertion on the thermal conductivity of a base fluid, thus promoting an enhancement of the single-phase forced convection HTC. Subsequently, Choi and Eastman [8] designated such solutions of nanoparticles dispersed in base fluids as *nanofluids*, and evaluated the feasibility of their application as thermal fluids. These authors conducted a theoretical investigation in which they stated that the thermal conductivity of nanofluids, hence the convective HTC, would be significantly enhanced due to the high thermal conductivity of metallic nanoparticles, which can be higher than that of conventional fluids by up to two orders of magnitude. Triggered by this work, a large number of research groups dedicated to study thermophysical properties of nanofluids have arisen around the world.

Pak and Cho [19] produced Al_2O_3- and TiO_2-loaded water-based nanofluids and evaluated variations in viscosity and HTC for internal forced convection. These authors verified an augmentation on both HTC and pressure

drop for fixed values of Reynolds number. Pak and Cho [19] also indicated higher increments in the fluid viscosity with addition of nanoparticles than the values predicted by correlations from the literature. Lee et al. [20] assessed the thermal conductivity of nanofluids containing oxide nanoparticles, and noticed reasonable agreement between their experimental data for fluids containing micrometer-sized clusters and Hamilton–Crosser correlation [21], while the thermal conductivity of fluids containing nanometer-sized clusters was underestimated by the same correlation. Xuan and Li [22] indicated that increments in thermal conductivity and dynamic viscosity were directly related to concentration of nanoparticles in nanofluids, corroborating previous results. These authors also pointed out that shape and dimensions of nanoparticles could significantly alter nanofluids transport properties, such that a careful preparation procedure of the nanofluids should be carried out, because particles clusters will modify the effective particles dimensions within the fluids. They indicated ultrasonication and the use of surfactants as viable procedures to obtain stable solutions with dispersed particles.

Later on, many other studies regarding the thermal conductivity of nanofluids were conducted, and large discrepancies between experimental data acquired by distinct research groups for similar nanofluids were noticed. An example is the comparison between the data of Li and Peterson [23] and Das et al. [24], which found increments in the thermal conductivity of 35 and 18%, respectively, for DI-water nanofluids containing 4% of CuO nanoparticles. In this context, Boungiorno et al. [25] coordinated an investigation involving 34 independent research groups that employed distinct fabrication and thermal conductivity characterization methods for nanofluids. According to this work, there is no exceptional augmentation of thermal conductivity related to the addition of nanoparticles, and this property can be satisfactorily predicted by existing correlations. Motivated by applications in heat exchangers, Tertsinidou et al. [26] measured transport properties of various nanofluids composed by water and ethylene–glycol as base fluids. Then, based on the measured values of the nanofluid properties, they analyzed variations in the effective heat transfer coefficient predicted by correlations, concluding that the combined effects of increased thermal conductivity and viscosity are usually not advantageous to the overall thermal performance.

Efforts on investigations concerning phase-change heat transfer behavior of nanofluids began in the early 00's. Das et al. [27] studied pool boiling of water/Al_2O_3 nanofluids and observed that the addition of Al_2O_3 nanoparticles to water is detrimental to the HTC. Research on flow boiling was headed by Faulkner et al. [28], who aimed for electronics cooling applications and reported an increase in HTC of nanofluids compared to the base fluid. You et al. [29] draw boiling curves for nanofluids and found significant enhancement of the critical heat flux (CHF) of nanofluids compared to deionized water. Most recently, Buongiorno [30] stated that the use of nanofluids is mostly indicated for applications that require drastic increases in CHF. Such conclusions have led to investigations toward the influence of nanofluids and surface nanostructuring on CHF and HTC, which has been widely investigated in recent works [31–34]. Since there is no consensus yet on the role of nanofluids in heat transfer, various aspects that can influence the behavior of nanofluids and their thermophysical properties were reviewed and are presented in the next sections.

3 Preparation, stabilization, and characterization of nanofluids

It is well known that the heat transfer coefficient is influenced by the transport properties of the fluid either for single- or two-phase flows. Thus, the characterization of such properties is an essential task if one wants to investigate the physical mechanisms that are responsible for changes in heat transfer rates when nanoparticles are added to base fluids. According to the literature, the transport properties can be significantly altered by the employed fabrication and stabilization methods, as endorsed by Babita et al. [9], and it is important that transport properties are adequately measured, in order to guarantee that the obtained values correspond to homogeneous solutions with known sizes, shapes, and targeted concentrations of particles. In this sense, techniques for preparation, stabilization, and characterization of nanofluids are discussed next.

3.1 Preparation

In general, nanofluids preparation can be divided into one- or two-step methods. In one-step methods, nanoparticles grow in the base fluid, usually through chemical reactions, while in two-step methods they are added to the base fluid and subsequently dispersed using a homogenization technique. A detailed analysis of nanofluids fabrication methods was presented by Das et al. [35], where they concluded that two-step methods is less efficient in terms of producing stable nanofluids, if compared to one-step methods. Stabilization of nanofluids can be improved by the use of surfactants, but they can modify many properties of the solution and, consequently, affect the heat transfer behavior, especially for heat transfer mechanisms involving nucleate boiling. Although nanofluids produced by two-step methods are generally less stable, such methods became popular because they are easily implemented and more flexible, since nanopowders of numerous materials

are commercialized and can be mixed into any fluid. It should be remarked that two-step methods also suit industrial applications better than one-step methods, due to faster preparation and up-scalable fabrication [36].

3.2 Stabilization

Nanofluids can be treated as colloids, which are dispersions with one of its components with dimensions between 1 nm and 1 μm. If the characteristic dimension of the dispersed phase is smaller than a critical radius (r_c), no sedimentation will occur because gravitational effects are surpassed by Brownian movements. Nevertheless, nanoparticles' surface energy increases for smaller dimensions [37], and the probability of aggregation rises, so the effective size of dispersed particles can be much larger than that of a single particle, resulting in sedimentation that characterizes unstable nanofluids. Ghadimi et al. [36] indicated that sedimentation velocity (v) in a suspension of particles that are larger than the critical radius is related to the balance of forces of a single particle suspended in a continuous medium. For a stationary fluid, according to Stokes' Law, it is given by:

$$v = \frac{2r_{\mathrm{np}}^2(\rho_{\mathrm{np}} - \rho_{\mathrm{bf}})g}{9\mu_{\mathrm{bf}}} \quad (1)$$

where r_{np} is the particle radius, ρ_{np} and ρ_{bf} are densities of particle and base fluid, respectively, g is acceleration due to gravity, and μ_{bf} is the viscosity of the base fluid. Based on Eq. (1), sedimentation velocity can be reduced if the effective dimensions of dispersed phase are diminished, the viscosity of the base fluid is increased, or density values of both components are similar [38].

Sedimentation can be avoided by the addition of surfactants to the mixture, since they reduce surface energy, thus promoting particle repulsion and inhibiting agglomeration [36, 39, 40]. Ghadimi et al. [36] discuss that colloids with a pH close to the isoelectronic point are less stable; thus, pH control is another way to improve nanofluids' stability. Naturally, if the charges surrounding the nanoparticles are chemically controlled, repulsion between particles can be assured, and thus, agglomeration and consequent sedimentation are prevented [36, 41–43]. Beck et al. [44] reported stabilization improvement by adding HCl to Al_2O_3 + water/ethylene–glycol nanofluids in order to reduce the pH of the solution to 4, avoiding the isoelectronic point (pH = 7). Oliveira et al. [45] reported stable behavior of water-based nanofluids containing up to 0.1% in volume of PVA-treated TiO_2 nanoparticles. Finally, another way of obtaining stable nanofluids through two-step methods is to work with low volumetric concentrations of nanoparticles (< 1%), as suggested by Zhang et al. [46]. As an example, Esfahani et al. [47] worked with mineral oil-based nanofluids prepared by a high-pressure homogenization method containing up to 0.05% in volume of silver, copper, or titanium oxide nanoparticles with no surfactants, and reported highly stable solutions even for 10 days after their preparation.

3.3 Characterization

Based on their experimental data [11, 12, 48], authors stated that nanofluids properties are badly predicted by established correlations commonly employed to calculate properties of blends containing micrometer-sized particles. These authors usually relate such unpredicted behaviors to interactions that are not relevant when larger-scale particles are taken into account, like Brownian movements and thermophoresis. To this date, no general behavior of nanofluids has been described yet, but it is a consensus that particles movements and interfacial effects significantly influence the transport behavior of nanofluids [17].

3.3.1 Thermal conductivity

Increments in thermal conductivity were pointed by Choi et al. [49] as the main reason for heat transfer coefficient intensification on single-phase forced convection of nanofluids. According to Lomascolo et al. [10], this is the reason for the existence of so many works dedicated to measuring the thermal conductivity of nanofluids and relating it to variations in the heat transfer coefficient. Since thermal conductivity value of the dispersed phase is generally two orders of magnitude higher than that of base fluid, even the addition of small amounts of nanoadditives could result in significant augmentation of nanofluids thermal conductivities [50–52].

There are many parameters that influence the variation of the thermal conductivity of a base fluid by the addition of a dispersed phase, e.g., materials properties, size and geometry of the solid phase, solution concentration, interaction between both phases, and temperature. It is observed that the increment in the thermal conductivity of the nanofluid is directly related to the thermal conductivity (k) of the nanoparticle material. This is verified by a comparison between solutions containing metal oxide inclusions [24, 47, 53, 54] and metallic additives [47, 53, 55, 56], with the latter presenting higher thermal conductivity values. Among these authors, Murshed et al. [53] observed that the presence of 1% in volume of alumina nanoparticles (k = 30 W/m K) in ethylene–glycol and engine oil base fluids resulted in an augmentation of 10% in thermal conductivity, whereas the thermal intensification caused by the same volume of aluminum nanoparticles (k = 204 W/m K) was 20%. Esfahani et al.

[47] also observed greater thermal conductivity enhancement in mineral oil-based nanofluids containing highly heat conducting fillers, like carbon nanotubes or silver, than nanofluids loaded with TiO_2 nanoparticles.

Although there are many aspects regarding the mechanisms that influence nanofluids transport properties, it is a consensus that the thermal conductivity of a solution increases with increasing nanoparticles volumetric concentration. Such statement is valid considering that particles with higher conductivity are added to the base fluid, as highlighted in the broad literature review on conductive, convective, and radiative heat transfer of nanofluids conducted by Lomascolo et al. [10]. Many authors reported linear increments in thermal conductivity with rising volumetric concentration of spherical nanoparticles [20, 24, 53, 54, 57–59]. Some authors observed that the intensification of the thermal conductivity of a base fluid promoted by cylindrical nanoparticles is higher than that promoted by spherical nanoparticles [53, 54, 60]. They also mentioned that for cylindrical nanoparticles the variation of the thermal conductivity with nanoparticle concentration follows an asymptotic behavior, presenting higher gradients for smaller volumetric concentrations [45, 47].

Lomascolo et al. [10] also stated that size effects on nanofluids transport properties are yet to be cleared, since distinct research groups observed different trends. Beck et al. [44] verified a reduction in thermal conductivity with decreasing particles diameter, especially for particles smaller than 50 nm. Feng et al. [61] concluded that lower thermal conductivity augmentation caused by smaller particles is a consequence of agglomeration. Contrarily to these investigations, Chopkar et al. [62] and Colangelo et al. [63] observed higher thermal conductivity intensification for nanofluids containing smaller particles, as was also noted by Mintsa et al. [64] for nanofluids at 48 °C. Nevertheless, for 20 °C, no major influence of nanoparticle size on thermal conductivity of nanofluids was detected by Mintsa et al. [64]. Such behaviors could be related to the temperature effect on Brownian motion and particles agglomeration [65].

Effects of temperature on nanofluids thermal conductivity have also been investigated, and, based on available data in the literature, Lomascolo et al. [10] inferred that the results obtained by independent research groups can rarely be employed to quantify the temperature influence in nanofluids thermal conductivity, since other important experimental parameters are usually distinct. Some authors indicate an augmentation of thermal conductivity with temperature [23, 24, 45, 53, 66, 67], while others verified no clear temperature effects [68] or even a reduction in thermal conductivity with rising temperature [12].

It is usual to find comparisons in the literature between experimental data and correlations that predict the thermal conductivity of heterogeneous materials. One of the most cited is the Maxwell's model [69], which was proposed for suspensions of non-interacting spherical particles dispersed in a continuous medium, and is given by:

$$k_{\mathrm{nf}} = \frac{\alpha + 2 + 2(\alpha - 1)\phi}{\alpha + 2 - (\alpha - 1)\phi} k_{\mathrm{bf}}, \tag{2}$$

where α is the thermal conductivity ratio between nanoparticles and the base fluid,

$$\alpha = {k_{\mathrm{np}}}/{k_{\mathrm{bf}}}$$

and ϕ is the volumetric concentration of the suspension. Another commonly cited correlation was proposed by Hamilton and Crosser [21], who extended Maxwell's model to suspensions containing cylindrical particles by including a configuration factor (n) into the expression, as follows:

$$k_{\mathrm{nf}} = \frac{\alpha + (n-1) + (n-1)(\alpha - 1)\phi}{\alpha + (n-1) - (\alpha - 1)\phi} k_{\mathrm{bf}}, \tag{3}$$

where

$$n = \frac{3}{\psi}, \tag{4}$$

and ψ is the sphericity, defined as the ratio between the surface area of a sphere with the same volume of one particle and the surface area of the particle. For spherical particles, $\psi = 1$ and $n = 3$, thus Hamilton–Crosser correlation turns into Maxwell's model.

Nan et al. [70] proposed a model for predicting the thermal conductivity of suspensions of particles within a fluid, considering the existence of interfacial thermal resistance between the dispersed and continuous phases and variations in particles geometries. For the limiting case of interest, where the dispersed phase is composed by spherical particles, Nan's model is given by:

$$k_{\mathrm{nf}} = \frac{\alpha + 2 + 2(\alpha - 1)\phi + 2\alpha(1 - \phi)\frac{R_{\mathrm{bd}} k_{\mathrm{bf}}}{r_{\mathrm{np}}}}{\alpha + 2 - (\alpha - 1)\phi + \alpha(2 + \phi)\frac{R_{\mathrm{bd}} k_{\mathrm{bf}}}{r_{\mathrm{np}}}} k_{\mathrm{bf}} \tag{5}$$

where R_{bd} is the interfacial thermal resistance between both phases and r_{p} is the particle radius. If $R_{\mathrm{bd}} = 0$, the interaction between both phases is perfect and Nan's model reverts to Maxwell's model. Since the interfacial thermal resistance is always positive, the effective thermal conductivity calculated by Eq. (5) will be lower than that predicted by Maxwell. Nevertheless, Maxwell's model usually underestimates thermal conductivity values of nanofluids, which suggests that there are significant heat transfer mechanisms that are being neglected in such calculations. Many authors compared their experimental data on thermal conductivity of nanofluids with Hamilton–Crosser correlation [11, 54, 71, 72], and the observed

inaccuracies were attributed to nanoscale-related effects, such as Brownian motions, which were not considered in this correlation because they have no significance when larger particles are employed [11, 48].

As already mentioned, in order to investigate possible reasons for the extraordinary heat transfer capabilities of nanofluids reported by some authors, Buongiorno et al. [25] performed a benchmark study, where seven distinct nanofluids were characterized by 34 independent research groups. These authors concluded that the thermal conductivity enhancement obtained by the addition of nanoparticles to a fluid increases linearly with rising volumetric concentration and aspect ratio, and is inversely related to the thermal conductivity of the base fluid. It should be remarked that no abnormal increment in thermal conductivity was reported in this investigation, and Nan's model [70] gave satisfactory predictions of the thermal conductivity measurements from independent laboratories.

Figure 1 shows a comparison between the predictive methods for the thermal conductivity of Hamilton and Crosser [21] and Nan et al. [70]. In this figure, it is observed that the interfacial thermal resistance plays a role of reducing the increment in the thermal conductivity of the nanofluid in relation to the base fluid. It is also noticeable that the predictions are similar when the interfacial thermal resistance is null and if spherical nanoparticles are considered.

3.3.2 Viscosity

Dynamic viscosity (μ) is an important transport property of fluids, since it is related to their resistance to deformation and is usually defined as the ratio between shear stress and velocity gradient or shear strain [73]. According to Mena et al. [74], nanofluids containing less than 13% in volume of particles behave as Newtonian fluids, i.e., their viscosity is independent on shear strain, thus can be determined through

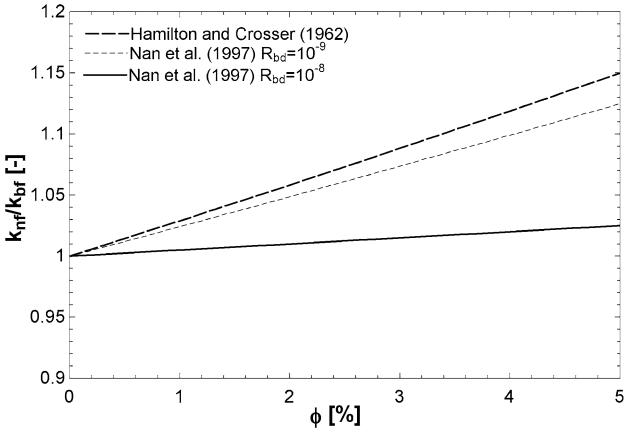

Fig. 1 Comparison between methods for predicting thermal conductivity values of nanofluids containing spherical Al_2O_3 nanoparticles with $d_{np} = 20$ nm

the slope of the straight line that relates shear stress versus shear strain of the fluid. If compared to thermal conductivity investigations, there are relatively few works related to the rheological behavior of nanofluids [36]. In general, viscosity of a base fluid is increased with the addition of nanoparticles [12, 45, 53, 57, 74–76], and therefore, the required pumping power for a given mass flow rate in a channel is raised. This behavior is in accordance with Reynolds–Colburn analogy, which states that increases in heat transfer are associated with rise in pressure loss.

Masuda et al. [12] observed an augmentation of 60% in the base fluid viscosity for nanofluids containing around 5% in volume of nanoparticles, while Wang et al. [75] and Murshed et al. [53] reported increments in viscosity of up to 80% for similar concentrations. Murshed et al. [53] employed surfactants in their nanofluids and stated that distinct dispersion techniques will result in solutions with different viscosities due to the size of particles agglomerates. Effects of particles size on viscosity of DI-water + Al_2O_3 nanofluids were investigated by Motta [57], who noticed increases in viscosity for smaller particles and higher concentrations of nanofluids. The viscosity of nanofluids containing 1% in volume of 20–30 nm Al_2O_3 nanoparticles has risen 55%, while that of nanofluids containing 1% of 15 nm Al_2O_3 nanoparticles presented augmentations of up to 90%.

Rises in dynamic viscosity were verified by Mena et al. [74] and Nguyen et al. [76] for lower temperatures and higher concentrations of nanoparticles. Besides, Nguyen et al. [76] also observed instabilities in nanofluids properties, which they defined as hysteresis, at temperatures above a certain threshold, named by the authors as critical temperature. Ghadimi et al. [36] stated that such behavior is a limiting aspect for enhancing heat transfer with nanofluids, since their properties may present unexpected variations, which results in inaccurate predictions of heat transfer and pressure loss coefficients. The shape of the dispersed particles can also alter nanofluids' viscosity. Timofeeva et al. [77] noticed that dispersions containing cylindrical nanoparticles were more viscous than dispersions containing the same concentration of spherical nanoparticles. These authors suggested that the use of cylindrical nanoparticles in potential applications is limited due to higher pressure drops, if compared to less viscous fluids, besides higher complexity in fabrication, thus being more expensive.

In the literature, dynamic viscosity of nanofluids is satisfactorily predicted by Einstein's equation [78–80], which is given by:

$$\mu_{nf} = (1 + 2.5\phi)\mu_{bf}, \tag{6}$$

where μ_{nf} and μ_{bf} are viscosities of the nanofluid and the base fluid, respectively, and ϕ is the volumetric concentration of dispersed phase. Einstein [78] deduced such equation for a suspension of spherical particles in a viscous

medium by considering the dispersed energy of a viscous fluid flowing over a single particle and relating it to the necessary work to dislocate a particle in this medium. Since interactions between particles were not considered in this model, Ghadimi et al. [36] suggested it could only be used for nanofluids containing less than 2% in volume of particles. Various modifications to Einstein's model were proposed in the literature, aiming to extend the range of its applicability. Usually, such modifications are based on correction factors related to the effective particle size, to the organization of particles in the medium, and to the distances between particles. Brinkman [81] proposed the following relation for dispersions containing microparticles:

$$\mu_{\mathrm{nf}} = \frac{1}{(1-\phi)^{2.5}}\mu_{\mathrm{bf}} \tag{7}$$

while Lundgren [82] employed a Taylor series expansion and derived their correlation:

$$\mu_{\mathrm{nf}} = \left(1 + 2.5\phi + \frac{25}{4}\phi^2\right)\mu_{\mathrm{bf}}, \tag{8}$$

which returns to Einstein's equation, if the second-order term is neglected. Graham [83] modified the model proposed by Frankel and Acrivos [84], such that it would coincide with Einstein's equation for smaller dimensions of particles, resulting in the relation:

$$\mu_{\mathrm{nf}} = \left\{1 + 2.5\phi + 2.25\left[\frac{1}{\left(1+\frac{\lambda}{2r_{\mathrm{np}}}\right)}\right]\left[\frac{1}{\left(\frac{\lambda}{r_{\mathrm{np}}}\right)} - \frac{1}{\left(1+\frac{\lambda}{r_{\mathrm{np}}}\right)} - \frac{1}{\left(1+\frac{\lambda}{r_{\mathrm{np}}}\right)^2}\right]\right\}\mu_{\mathrm{bf}}, \tag{9}$$

where λ is the minimum spacing between particles, and r_{np} is the particles' radius.

A comparison between the presented correlations for predicting the viscosity of nanofluids is shown in Fig. 2. For low concentrations, no significant variations are observed, as expected, but they are more relevant as the concentration rises, especially for values higher than 5%.

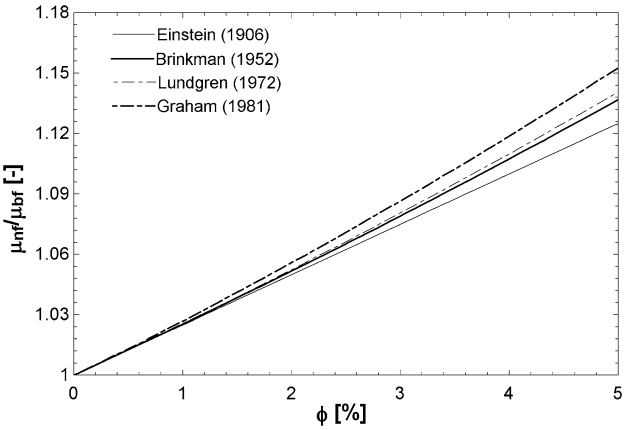

Fig. 2 Comparison between methods for predicting viscosity of nanofluids containing spherical nanoparticles with d_{np}=30 nm

3.3.3 Density and specific heat

Nanofluids density and specific heat are usually directly calculated by the rule of mixtures as a function of volumetric concentration of nanoparticles [85], as follows:

$$\rho_{\mathrm{nf}} = (1-\phi)\rho_{\mathrm{bf}} + \phi\rho_{\mathrm{np}}, \tag{10}$$

$$c_{\mathrm{p,nf}} = \frac{(1-\phi)\left(\rho c_{\mathrm{p}}\right)_{\mathrm{bf}} + \phi\left(\rho c_{\mathrm{p}}\right)_{\mathrm{np}}}{(1-\phi)\rho_{\mathrm{bf}} + \phi\rho_{\mathrm{np}}}, \tag{11}$$

where ρ_{nf} and $c_{\mathrm{p,nf}}$ are the density and specific heat of the nanofluid, ρ_{bf} and $(\rho c_{\mathrm{p}})_{\mathrm{bf}}$ are the density and volumetric heat capacity of the base fluid, and ρ_{np} and $(\rho c_{\mathrm{p}})_{\mathrm{np}}$ are the same properties of the nanoparticles. Variations of these properties according to volumetric concentration of nanoparticles for a solution containing Al_2O_3 nanoparticles dispersed in deionized water are illustrated in Fig. 3.

For the considered materials, specific heat decreases with concentration of nanoparticles, while density rises.

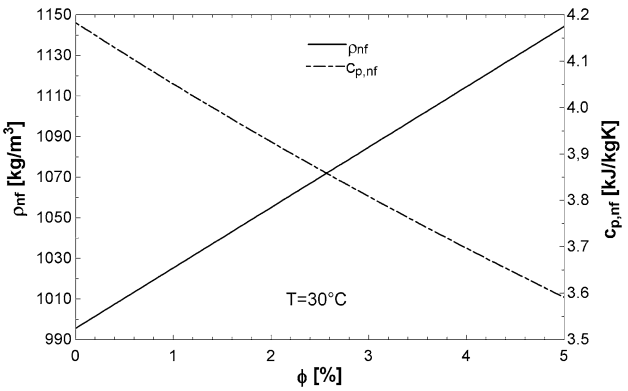

Fig. 3 Variations of density and specific heat due to volumetric concentration of alumina nanoparticles dispersed in deionized water

This increase in density should result in reductions in pressure drop for a fixed mass flow rate, since the flow velocity decreases for higher densities. However, this decrease in pressure drop is not verified, due to the significant viscosity augmentation. In addition, the decrease in specific heat implies that, for single-phase flow and for fixed values of mass flow rate and heat flux, larger temperature gradients will be obtained along the flow path when the nanofluid is heated or cooled, in comparison with the base fluid.

4 Single-phase flow of nanofluids

Most investigations regarding nanofluids applications are focused on single-phase flow of nanofluids. Studies concerning in-tube single-phase forced convection of nanofluids are summarized in Table 1. This table shows a dominance of water-based nanofluids, while various materials were employed as dispersed phase, e.g., graphite, graphene, copper, alumina, hematite, magnetite, titania, zinc oxide, carbon nanotubes, among others. Other fluids also used as continuous media were: transmission oil, mixtures of synthetic oils, water + ethylene–glycol, water + carboxymethyl cellulose, and water + cetyl-trimethyl-ammonium chloride. Tests were generally performed at temperatures close to environmental conditions, and the diameters of the channels varied between 50 μm to 16 mm.

Generally, studies indicate intensification of the HTC due to the addition of nanoparticles to base fluids. Nevertheless, this trend was not observed by some researchers [91, 103, 110, 112, 117]. Ding et al. [91] reported a decrease in the HTC for Reynolds numbers around 135 for nanofluids containing diamond nanoparticles dispersed in ethylene–glycol with surfactants to improve their stability. In a recent work, Chougule and Sahu [108] observed that, in comparison with the pure base fluid, the HTC of nanofluids containing surfactants presented less increase than nanofluids without surfactants, suggesting that the presence of surfactants in nanofluids may cause a degradation of the HTC. Gómez et al. [117] studied water nanofluids containing silver nanoparticles and single-walled carbon nanotubes (SWCNT), and verified increases of up to 7% in the HTC with augmentations of up to 13% in pumping power for silver-loaded nanofluids, while for SWCNT the heat transfer coefficient presented only decreases of up to 17% and increases in pumping power that reached 25%, in comparison with the base fluid.

Although Utomo et al. [103] reported that the thermal conductivity of a base fluid increases with the addition of nanoparticles, no significant variations in the HTC were observed by them for Reynolds numbers varying from 520 to 1080. For Reynolds numbers lower than 1500, Karimzadehkhouei et al. [110] did not observe significant variations of the HTC either, and they attributed the observed increments for Reynolds numbers greater than 1500 to the intensification of particles movements associated with turbulence effects. Li et al. [112] noticed that the HTC increased for nanoparticles mass fraction (ϕ_m) equal to 2.5%, while the HTC decreased for ϕ_m = 5%. According to the authors, such behavior suggests the existence of an optimum concentration of particles in the nanofluid, associated with a maximum heat transfer coefficient. A similar conclusion was presented by Azmi et al. [107], although the HTC in their study has only risen with increasing nanoparticles concentration.

Many authors in the literature reported increments of the HTC that surpass what would be expected solely by thermal conductivity augmentation [19, 66, 72, 85, 87, 88, 90, 91, 93, 94, 96, 98, 99, 102, 104, 107, 108, 111, 115, 116, 118]. Some of these authors performed their experiments for turbulent flows [19, 85, 87, 90, 98, 99, 102, 107, 108, 111, 115, 116], in which the HTC depends on density, dynamic viscosity, thermal conductivity, specific heat, channel diameter, and flow velocity, according to Dittus–Boelter correlation, written in terms of transport properties as follows:

$$h = 0.023\rho^{0.8}V^{0.8}d^{-0.2}\mu^{-0.4}k^{0.6}c_{\mathrm{p}}^{0.4}. \quad (12)$$

As already discussed, the addition of nanoparticles to base fluids is responsible for raising density, thermal conductivity, and viscosity, while diminishing the specific heat. Previous investigations show that changes in density and specific heat of nanofluids obey the rule of mixtures, and variations of thermal conductivity and viscosity are much more prominent. In addition, for the same mass flow rate, an increase in density will result in a decrease in fluid velocity of the same magnitude. Based on these observations and analyzing the exponents of Eq. (12), it is possible to infer that the thermal conductivity and viscosity are the main transport properties responsible for alterations in the HTC, if mechanisms related to particles movements are neglected. In this context, increments in the HTC for turbulent single-phase flow that are higher than the predicted values considering the thermal conductivity augmentation indicate the existence of additional mechanisms responsible for improving heat transfer that are generally neglected, like the movement of nanoparticles due to turbulence effects. Heyhat and Kowsary [119] conducted a similar analysis for laminar flows, in which Brownian movements and thermophoresis were responsible for particles motion, and thermal diffusion was enhanced by the migration of nanoparticles from regions closer to the wall to the center of the channel.

Table 1 Summary of experimental conditions and results for heat transfer coefficients of nanofluids on single-phase internal forced convection

Authors	Preparation method	Base fluid + nanoparticle/ϕ	d_h/surface material	Reynolds number	Effect on HTC
Pak and Cho [19]	Two steps + variation of the pH	Water + Al_2O_3/1.34–2.78% (vol)	10.66 mm/stainless steel	10^4–10^5	↑
		Water + TiO_2/0.99–3.16% (vol)			↑
Li and Xuan [86]	Two steps + surfactant	Water + Cu/0.3–2% (vol)	10 mm/brass	800–25,000	↑
Xuan and Li [87]	Two steps + surfactant	Water + Cu/0.3–2% (vol)	10 mm/brass	10,000–25,000	↑
Wen and Ding [88]	Two steps + surfactant	Water + Al_2O_3/0.6–1.6% (vol)	4.5 mm/copper	500–2100	↑
Yang et al. [11]	–	Mixture of synthetic oils + graphite/2% (mass)	4.57 mm/–	5–110	↑
		Transmission oil + graphite/2–25% (mass)			↑
Heris et al. [89]	Two steps	Water + Al_2O_3/0.2–3% (vol)	6 mm/copper	650–2050	↑
		Water + CuO/0.2–3% (vol)			↑
Ding et al. [66]	Two steps + surfactant	Water + CNT/0.1–0.5% (vol)	4.5 mm/copper	800–1200	↑
Lee and Mudawar [80]	Obtained from manufacturer and diluted	Water + Al_2O_3/1–2% (vol)	341 μm/copper	140–941	↑
He et al. [90]	Two steps + variation of the pH	Water + TiO_2/0.24–1.18% (vol)	3.97 mm/copper	900–5900	↑
Ding et al. [91]	Two steps + variation of the pH	Water + TiO_2*	3.97 mm/copper	50–450	↑
		Water + CNT*			↑
	Two steps + surfactant (diamond)	Water + titanate nanotubes*			↑
		Water + Diamond*			↓
		Ethylene–glycol + TiO_2*			↓
Willians et al. [92]	Obtained from manufacturer and diluted	Water + Al_2O_3/0.9–3.6% (vol)	9.4 mm/stainless steel	9000–63,000	↑
		Water + ZrO_2/0.2–0.9% (vol)			↑
Hwang et al. [93]	Two steps	Water + Al_2O_3/0.01–0.3% (vol)	1.812 mm/stainless steel	500–800	↑
Jung et al. [94]	Two steps	Water + Al_2O_3/0.6–1.8% (vol)	50. 100 and 66.67 μm/silicon	5–300	↑
		Water/ethylene–glycol + Al_2O_3/0.6–1.8% (vol)			↑
Rea et al. [95]	Obtained from manufacturer and diluted	Water + Al_2O_3/0.6–6% (vol)	4.5 mm/stainless steel	140–1888	↑
		Water + ZrO_2/0.32–1.32% (vol)			↑
Anoop et al. [96]	Two steps + variation of the pH	Water + Al_2O_3/1–6% (mass)	4.75 mm/copper	550–2100	↑
Amrollahi et al. [97]	Two steps	Water + CNT/0.1–0.25% (mass)	11.42 mm/copper	1500–4800	↑
Liu and Liao [98]	Two steps + variation of the pH	Water/CTAC + CNT/0.5–4% (mass)	25.6 mm/copper	5000–50,000	↑
Asirvatham et al. [99]	Two steps	Water + Ag/0.3–0.9% (vol)	4.3 mm/copper	1000–10,000	↑
Hojjat et al. [100]	Two steps	Water/CMC + Al_2O_3/0.1–1.5% (vol)	10 mm/stainless steel	8000–33,000	↑
		Water/CMC + TiO_2/0.1–1.5% (vol)			↑
		Water/CMC + CuO/0.1–1.5% (vol)			↑
Nasiri et al. [101]	Two steps	Water + Al_2O_3/0.1–1.5% (vol)	9 mm/stainless steel	4000–35,000	↑
		Water + TiO_2/0.1–1.5% (vol)			↑
Suresh et al. [102]	Two steps	Water + CuO/0.1–0.3% (vol)	4.85 mm/copper	2500–6000	↑
Utomo et al. [103]	Obtained from manufacturer and diluted	Water + Al_2O_3/2.4% (vol)	4.57 and 10 mm/stainless steel	520–1080	↔
		Water + TiO_2/2.4% (vol)			↑
Godson et al. [85]	Two steps	Water + Ag/0.3–0.9% (vol)	4.3 mm/copper	900–12,000	↑
Zhang et al. [46]	Obtained from manufacturer and diluted	Water + Al_2O_3/0.25– 0.77% (vol)	0.5 mm/*	500–2000	↑
Heyhat et al. [104]	Two steps	Water + Al_2O_3/0.1–2% (vol)	5 mm/copper	330–2200	↑

Table 1 (continued)

Authors	Preparation method	Base fluid + nanoparticle/ϕ	d_h/surface material	Reynolds number	Effect on HTC
Peyghambarzadeh et al. [105]	Two steps + variation of the pH	Water + CuO/0.15–0.65% (vol)	3.9 mm/Aluminum	50–1000	↑
		Water + Fe_2O_3/0.15–0.65% (vol)			↑
Sahin et al. [106]	Two steps	Water + Al_2O_3/0.5–4% (vol)	11.7 mm/ Aluminum	4000–20,000	↑
Azmi et al. [107]	Obtained from manufacturer and diluted	Water + TiO_2/0.5–3% (vol)	16 mm/copper	5000–25,000	↑
		Water + SiO_2/0.5–3% (vol)			↑
Chougule and Sahu [108]	Two steps + variation of the pH	Water + CNT/0.15–1%	5.22 mm/ Aluminum	9000–26,000	↑
	Two steps + surfactant				↑
Sun et al. [109]	Two steps + surfactant	Water + Fe_2O_3/0.1–0.4%	8.22 mm/copper	1000–2000	↑
Karimzadehkhouei et al. [110]	Two steps	Water + Al_2O_3/0.01–2% (mass)	0.502 mm/stainless steel	289–2190	↑ $Re > 1500$
		Water + TiO_2/0.01–3% (mass)			↔ $Re < 1500$
Gómez et al. [111]	Two steps	Water + CNT/0.12–0.14% (vol)	6.78 mm/Brass	3500–18,500	↑
Li et al. [112]	Two steps	Ethylene–glycol/Water + ZnO/2.5 and 5% (mass)	8 mm/stainless steel	1000–4000	↑ Ø = 2.5% ↓ Ø = 5%
Akhavan-Zanjani et al. [72]	One step + surfactant	Water + Graphene/0.005–0.02% (vol)	4.2 mm/copper	600–1850	↑
Colla et al. [113]	Obtained from manufacturer and diluted	Water + Al_2O_3/1–3% (vol)	12.66 mm/stainless steel	4000–14,000	↑
Selvam et al. [114]	Two steps + surfactant	Ethylene–glycol/Water + Ag/ 0.05–0.45% (vol)	4.3 mm/*	500–12,000	↑
Sundar et al. [115]	Two steps + surfactant	Water + Fe_3O_4–CNT nanocomposite/0.1 and 0.3% (vol)	18 mm/copper	3000–22,000	↑
Zarringhalam et al. [116]	Two steps	Water + CuO/0.0625–2% (vol)	6.15 mm/copper	2900–18,500	↑
Gómez et al. [117]	Two steps	Water + SWCNT/0.03, 0.05 and 0.2% (vol)	6.35 mm/Brass	4500–18,500	↓
		Water + Ag/0.1, 0.3 and 0.5% (vol)		6000–20,500	↑
Moreira et al. [118]	Two steps	Water + Al_2O_3 (20–30 nm)/0.001, 0.01 and 0.1% (vol)	1.1 mm/stainless steel	570–1900	↑
		Water + Al_2O_3 (40-80 nm)/0.001, 0.01 and 0.1% (vol)			

↑ increase;↓ decrease; ↔ non-noticeable effect; * not indicated by the authors

Heat transfer behavior of nanofluids under laminar conditions was investigated for developing [66, 88, 94, 96] and fully developed flows [72, 91, 93, 104]. In developing flows, nanoparticles migration can occur due to shear gradients, thermophoresis, and Brownian motion, resulting in a higher increase in the HTC than the thermal conductivity augmentation alone would cause [118]. In fact, Heyhat and Kowsary [119] concluded that energy transport due to nanoparticles migration is enough to justify the unexpected rises of the HTC, and Hwang et al. [93] verified that thermophoresis and Brownian motions are the main mechanisms responsible for particles movements, based on dimensional analysis of nanoparticles migration in a continuous medium. Moreira et al. [118] compared their experimental results with numeric simulation, indicating that just the Brownian motion and thermophoresis are not capable of promoting the increment in the HTC displayed according to their experimental data. These authors

indicated that some other unaccounted phenomenon related to the dimensions of the particles could be responsible for the heat transfer enhancement.

Interactions between base fluids and nanoparticles, especially due to Brownian motion, were pointed as the main reasons for unexpected growth of HTC in many investigations [85–87, 91, 93, 98, 99, 101, 104, 108, 111, 115]. Gómez et al. [111] and Sundar et al. [115] indicate that carbon nanotubes with high aspect ratio favor Brownian movements. According to Li and Xuan [86] and Xuan and Li [87], these random movements of nanoparticles homogenize temperature profiles in the cross section, and consequently increase heat transfer in regions close to the channel walls. These authors also highlighted the importance of an adequate nanoparticles choice, in order to promote reasonable thermal conductivity intensification with minimum variation of viscosity. This results in reduced turbulence suppression effects and minimum variation of pressure drop, effects that are related to increments of viscosity.

In addition to nanoparticles migration, Heyhat et al. [104] and Hwang et al. [93] revealed that fluctuations of the velocity profile could also act as a mechanism to intensify heat transfer. Nasiri et al. [101] and Godson et al. [85] indicated the alteration of base fluids properties due to the addition of nanoparticles as another mechanism responsible for enhancing heat transfer, besides Brownian motions. Ding et al. [66] and Liu and Liao [98] evaluated the effects of temperature and nanofluid concentration in the HTC, and concluded that sensitivity to temperature variations is higher than to the concentration. Referring to Buongiorno [120] and Liu and Liao [98] explained that temperature raises result in escalation of the Brownian motions, thus improving heat transfer. Heris et al. [89] observed superior augmentation of HTCs measured in experiments with Al_2O_3-loaded nanofluids than with CuO nanofluids, even though nanofluids containing CuO presented higher thermal conductivity. This behavior was attributed to the higher viscosity of CuO-loaded nanofluids.

Some researchers suggested the reduction in boundary layer as the mechanism responsible for increments in heat transfer, since it extends the developing length where heat transfer is more intense [66, 88, 102, 114]. Suresh et al. [102] related such reduction to particles movement and to the higher thermal conductivity, which could be associated with diminishment of Prandtl number. Ding et al. [66] claimed that thermal conductivity of nanofluids is higher under dynamic shear than under quiescent conditions. He et al. [90] hypothesized that the possible migration of particles to the center of the channel, also speculated by Wen and Ding [88], could suppress the effects of nanoparticles dimensions in the HTC for flows with Reynolds number varying from 900 to 5900. Ding et al. [91] also attributed to particles migration effects, reductions in the HTC observed for ethylene–glycol nanofluids at Reynolds numbers close to 135.

Maximum intensifications of the HTC along the developing region were reported by some authors [66, 72, 80, 88, 91, 96], which corroborate the hypothesis that the main heat transfer enhancement mechanism is linked to changes in the thermal boundary layer due to the presence of nanoparticles. Yang et al. [11] analyzed the effects of distinct base fluids with similar transport properties in the HTC of single-phase flow of graphite-loaded nanofluids. These authors identified some differences in the heat transfer behavior of nanofluids containing the same amount of graphite and at the same conditions, which should be related to the interaction between particles and the distinct fluids.

He et al. [90] investigated laminar and turbulent flows, and noticed more prominent rising of the HTC for turbulent flows with the addition of nanoparticles. They also stated that even though nanoparticles dimensions may alter the thermal conductivity, no meaningful variations were observed in the HTC. On the other hand, Anoop et al. [96] noted higher HTC enhancements for nanoparticles with smaller dimensions. Willians et al. [92] and Rea et al. [95] concluded that the HTC for turbulent and laminar flows of nanofluids, respectively, can be adequately predicted by correlations for pure fluids, once the transport properties of the nanofluids are experimentally evaluated.

Differently than most authors, some researchers noticed increases in the convective HTC that were compatible to the observed increments in thermal conductivity [11, 92, 95, 97, 113, 114]. On the other hand, Amrollahi et al. [97] reported lower increments in the HTC than expected for turbulent flows, based on their experimental data. Few groups performing studies on single-phase forced convection of nanofluids presented no thermal conductivity data of the evaluated nanofluids [46, 86, 101, 105, 109].

5 Boiling of nanofluids

Heat transfer processes involving phase change are known to provide much higher heat transfer coefficients than single-phase heat transfer. In addition, during phase change, temperature variation is minimum and directly associated with pressure variations. These two aspects turn boiling heat transfer into interesting solutions for applications in which high heat fluxes must be dissipated and temperature gradients are undesirable, since they promote thermal stresses and efficiency reduction. In general, there is no consensus among independent studies on whether the use of nanofluids is advantageous or not, but there is an

agreement on the role of nanoparticles in modifying surface properties due to particle deposition during boiling processes. However, the real effects of deposition are not clear yet, and some authors have pointed it as beneficial to increase heat transfer, while others observed deleterious effects. In this section, the literature concerning the use of nanofluids in boiling processes for surface nanostructuring and the behavior of these fluids on pool and flow boiling is discussed.

5.1 Deposition of nanoparticles and effects on surface wettability

Nucleate boiling promotes deposition of particles on the surface, changing its morphological characteristics and, consequently, affecting bubble nucleation and growth. Particles deposition is intensified around bubble nucleation sites, close to the triple contact line, where the evaporation is intense, causing local increases in particles concentration as shown in Fig. 4 [121, 122]. It was speculated that these local variations in particles concentration act in favor of particles collisions and consequent agglomeration, triggering deposition over the heated surface. A surface characteristic that is significantly modified by particles deposition and intimately related to nucleate boiling heat transfer behavior is the wettability. The wettability is associated with inundation of surface cavities; therefore, it can be linked to the required energy for activation of bubble nucleation sites. In general, nanoparticles deposition alters surface texture and energy [62, 123, 124], reducing contact angle, hence increasing wettability. Such behavior diminishes nucleate boiling heat transfer, because this involves increments of the necessary wall superheating for bubble nucleation. However, Souza et al. [125] revealed that the heat transfer coefficient for HFE7100 under confined and unconfined nucleate boiling on nanoparticles-covered surfaces could increase or decrease in comparison with the bare surface, depending on particles size and surface texture. These authors argued that the deposited layer containing 80-nm particles was thicker, with higher thermal resistance, and that these particles could block some cavities, reducing the number of active nucleation sites, while 10 nm particles increased the number of active nucleation sites, thus improving heat transfer.

Some authors verified that particles deposition affects more significantly surface wettability than its roughness [126–128]. In these works, substantial diminution of the contact angle was noticed for stainless steel and aluminum substrates after nanoparticles deposition. According to Buongiorno [30], such behavior occurs due to capillarity effects on the porous layer created by the deposition process. Figure 5 shows the difference of deionized water droplets deposited over a bare aluminum surface and over the same plate covered by a super-wetting porous layer produced by the deposition of alumina nanoparticles through nucleate boiling process [128]. This figure exhibits complete splashing of an 8 µl droplet over the coated surface, while a static droplet with contact angle of 67° is seen over the bare surface.

5.2 Pool boiling of nanofluids

Pool boiling of nanofluids has been extensively investigated over the last decade. Table 2 presents a survey of works regarding pool boiling of nanofluids. A major part of these studies involved water-based nanofluids, as also seen in Table 1 for single-phase tests, but some other base fluids were also employed, like: R141b, R134a + polyolester, R113 + VG68 oil, ethanol, and water + ethylene–glycol solutions. Again, various materials were used as dispersed

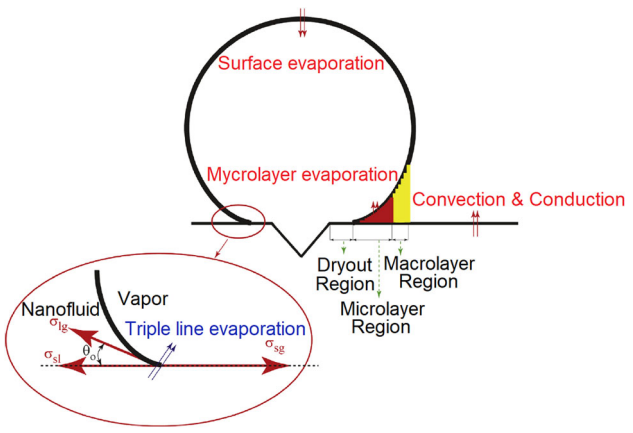

Fig. 4 Schematic diagram of heat transfer and expansion mechanisms during bubble growth [122]

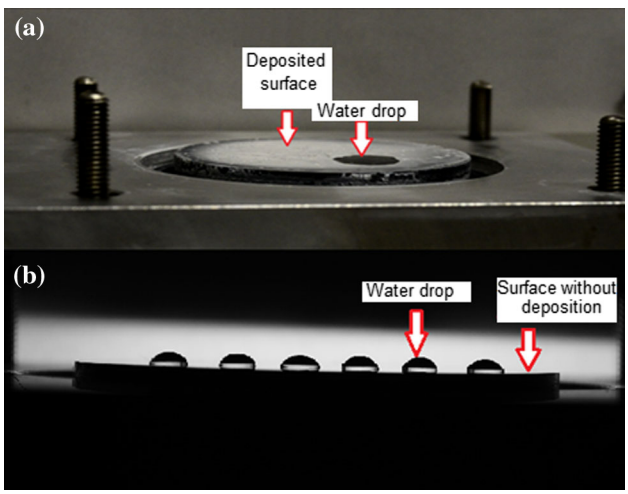

Fig. 5 Deionized water droplets deposited on an aluminum substrate covered by 20–30 nm Al_2O_3 nanoparticles (**a**) and on a bare aluminum surface (**b**)

Table 2 Summary of experimental conditions and results for investigations concerning pool boiling of nanofluids

Authors	Subject of study	Substrate material	Preparation method	Composition	Heater type/Dimensions	T/ϕ	Effect on HTC
Das et al. [27]	HTC	Stainless steel	Two steps	Water + Al_2O_3 (38 nm)	Block: horizontal cylinder/d = 20 mm	100 °C/0.1–4% (vol)	↓
Das et al. [129]	HTC	Stainless steel	Two steps	Water + Al_2O_3 (58.4 nm)	Block: Horizontal cylinder/d = 6.5 and 20 mm	100 °C/1–4% (vol)	↓
You et al. [29]	CHF	Copper	–	Water + Al_2O_3 [+]	Block: square horizontal flat surface/l = 10 mm	60 °C/0.001–0.05 (g/l)	↔
Vassallo et al. [130]	HTC, CHF	Nickel–Chromium	Obtained from manufacturer and diluted	Water + SiO_2 (15 and 50 nm)	Horizontal wire/L = 75 mm	100 °C/0.5% (vol)	↔
Wen and Ding [131]	HTC	Stainless steel	Two steps	Water + Al_2O_3 (10–50 nm)	Block: Circular horizontal flat surface/ d = 150 mm	100 °C/ 0.32–1.25% (vol)	↑
Bang and Chang [132]	HTC, CHF	Copper	Two steps	Water + Al_2O_3 (47 nm)	Block: rectangular horizontal flat surface/ 4 mm × 100 mm	100 °C/0.5–4% (vol)	↓
Park and Jung [133]	HTC	Copper	Two steps	R22 + CNT (d = 20 nm and L = 1 μm)	Tube: Horizontal cylinder/d_o = 19 mm, L = 152 mm	7 °C/1% (vol)	↑
				Water + CNT		100 °C/1% (vol)	↑
Narayan et al. [134]	HTC	Stainless steel	Two steps + variation of the pH	Water + Al_2O_3 (47 and 150 nm)	Tube: Vertical cylinder/–	Temperature not informed/ 0.5–2% (mass)	↑ * ↓ **
Liu et al. [135]	CHF	Copper	Two steps	Water + CuO (30 nm)	Block: Square horizontal grooved flat surface/ l = 40 mm, grooves: w = 0.5 mm, h = 0.8 mm	100, 70, 60 and 40 °C/0.1–2% (mass)	↑ Ø < 1% ↓Ø > 1%
Kim et al. [136]	CHF	Stainless steel	Obtained from manufacturer and diluted	Water + Al_2O_3 (110–210 nm)	Horizontal wire/d = 0.38 mm, L = 120 mm	100 °C/ 0.001–0.01% (vol)	↓
				Water + ZrO_2 (110–250 nm)			↓
				Water + SiO_2 (20–40 nm)			↓
Kim et al. [137]	Quenching	Stainless steel	Obtained from manufacturer and diluted	Water + Al_2O_3	Block: Spherical surface/d = 9.5 mm	100 °C/ 0.001–0.1% (vol)	↔
Chopkar et al. [62]	HTC	Copper	Two steps + surfactant	Water + ZrO_2 (20–25 nm)	Block: Circular horizontal flat surface/ d = 60.5 mm	100 °C/ 0.005–0.15% (vol)	↑ ↓ Ø = 0.15%
Trisaksri and Wongwises [138]	HTC	Copper	Two steps	R141b + TiO_2 (21 nm)	Block: Horizontal cylinder/d = 28.5 mm, L = 90 mm	200–500 kPa/ 0.01–0.05% (vol)	↓
Park et al. [139]	HTC, CHF	Copper	Two steps + surfactant	Water + CNT (d = 10–20 nm and L = 10–50 μm)	Block: Square horizontal flat surface/ l = 9.53 mm	60 °C/ 0.0001–0.05% (vol)	↓

Table 2 (continued)

Authors	Subject of study	Substrate material	Preparation method	Composition	Heater type/Dimensions	T/ϕ	Effect on HTC
Kedzierski and Gong [140]	HTC	Copper	Obtained from manufacturer and diluted	R134a/polyolester + CuO (30 nm)	Block: Rectangular horizontal flat surface/ 101.6 mm × 25.4 mm	7 °C/0.5–2% (mass)	↑
Suriyawong and Wongwises [141]	HTC	Copper	Obtained from manufacturer and diluted	Water + TiO_2 (21 nm)	Block: Circular horizontal flat surface/–	100 °C/ 0.00005–0.01% (vol)	↑ Ø < 0.0001%
		Aluminum					↑ Ø > 0.0001%
Kathiravan et al. [142]	HTC, CHF	Stainless steel	Two steps	Water + Cu (10 nm)	Block: Square horizontal flat surface/l = 30 mm	100 °C/0.25–1% (mass)	↓
Kwark et al. [121]	CHF	Copper	Two steps	Water + CuO (143 nm)	Block: Square horizontal flat surface/l = 10 mm	100 °C/0.001–1 (g/l)	↓
				Water + diamond (86 nm)			↓
				Water + Al_2O_3 (139 nm)			↓
Okawa and Kamiya [143]	CHF	Copper	–	Water + TiO_2 (21 nm)	Block: Circular horizontal flat surface/ d = 20 mm	100 °C/ 0.009–0.455 (g/l)	↓
Peng et al. [144]	HTC	Copper	Two steps	R113/oil VG68 + CNT (d = 15 and 80 nm. L = 1.5 and 10 μm)	Block: Circular horizontal flat surface/ d = 20 mm	47.6 °C/0.1–1% (mass)	↑
Liu et al. [145]	HTC, CHF	Copper	Two steps + variation of the pH	Water + CNT (d = 15 nm, L = 5–15 μm)	Block: Square horizontal flat surface/l = 40 mm	100 and 40 °C/ 0.5–4% (mass)	↑
Kedzierski [146]	HTC	Copper	Obtained from manufacturer and diluted	R134a/polyolester + Al_2O_3 (10 nm)	Block: Rectangular horizontal flat surface/ 101.6 mm × 25.4 mm	4.4 °C/0.5–2% (mass)	↑
Heris [147]	HTC	Stainless steel	Two steps	Water + Ethylene–glycol + CuO (40 nm)	Block: Horizontal cylinder/d = 7 mm	100 °C/0.1–0.5% (mass)	↑
Cieslinski and Kaczmarczyk [148]	HTC	Copper	Two steps	Water + Al_2O_3 (47 nm)	Tube: Horizontal cylinder/d_o = 10 mm, L = 100 mm	100 °C/0.01–1% (mass)	↔
				Water + Cu (48 nm)			↔
		Stainless steel		Water + Al_2O_3 (47 nm)			↓
				Water + Cu (48 nm)			↓
Huang et al. [149]	CHF	Nickel	Two steps	Water + TiO_2 (110–220 nm)	Horizontal wire/d = 0.3 mm, L = 50 mm	100 °C/0.01–1% (mass)	↓
Kathiravan et al. [150]	HTC	Stainless steel	Two steps	Water + CNT (d = 10–15 nm, length not verified)	Block: Square horizontal flat surface/ l = 5.5 mm	100 °C/0.25–1% (vol)	↑
			Two steps + surfactant				↑
Yang and Liu [151]	HTC, CHF	Copper	Two steps	Water + SiO_2 with functionalized surface (30 nm)	Block: Square horizontal flat surface/l = 40 mm	100 and 40 °C/ 0.5–2.5% (mass)	↑
				Water + SiO_2 (30 nm)			↓

Table 2 (continued)

Authors	Subject of study	Substrate material	Preparation method	Composition	Heater type/Dimensions	T/ϕ	Effect on HTC
Ahmed and Hamed [152]	HTC	Copper	Two steps	Water + Al_2O_3 (40–50 nm)	Block: Circular horizontal flat surface/ d = 25.4 mm	100 °C/ 0.01–0.5% (vol)	↑
Wen [153]	HTC	Copper	Two steps	Water + Al_2O_3 (20–150 nm)	Block: Square horizontal flat surface/l = 20 mm	100 °C/ 0.001–0.1% (vol)	↔ smooth surface ↑ rough surface
Kathiravan et al. [154]	HTC, CHF	Stainless steel	Two steps + surfactant	Water + Ag (15 nm)	Block: Square horizontal flat surface/l = 30 mm	100 °C/ 0.25–0.75% (vol)	↑
Kole and Dey [155]	HTC, CHF	Copper	Two steps	Ethylene–glycol + ZnO (120 nm)	Block: Horizontal cylinder/d = 15 mm	197 °C/ 0.35–2.6% (vol)	↑
Duangthongsuk et al. [156]	HTC	Copper	Obtained from manufacturer and diluted	Water + Al_2O_3 (120 nm)	Block: Horizontal cylinder/d = 28.5 mm, L = 90 mm	100 and 120 °C/ 0.00005–0.03% (vol)	↓
Shahmoradi et al. [157]	HTC, CHF	Copper	Two steps	Water + Al_2O_3 (40 nm)	Block: Circular horizontal flat surface/ d = 38 mm	100 °C/ 0.001–0.1% (vol)	↓
Shoghl and Bahrami [158]	HTC	Stainless steel	Two steps	Water + ZnO^+ Water + CuO^+	Block: Horizontal cylinder/d = 10.7 mm, L = 99.1 mm	100 °C/ 0.01–0.02% (mass)	↓ ↓
Raveshi et al. [159]	HTC	Copper	Two steps + surfactant	Water/Ethylene–glycol + Al_2O_3 (20–30 nm)	Block: Circular horizontal flat surface/ d = 40 mm	163 °C/0.05–1% (vol)	↑
Mohamadifard et al. [160]	HTC	Stainless steel	Two steps	Water/Ethylene–glycol + Al_2O_3 (20 nm)	Block: Horizontal cylinder/d = 7 mm	111 °C/0.1–0.5% (mass)	↑
Naphon and Thongjing [161]	HTC	Brass	Two steps	R141b + TiO_2 (21 nm)	Block: Horizontal cylinder/d = 12.7 mm, L = 42 mm	13.4–43.7 °C/ 0.01–0.075% (vol)	↓
				Ethanol + TiO_2 (21 nm)		61.4–88.5 °C/ 0.01–0.075% (vol)	↓
Cieslinski and Krygier [162]	HTC, CHF	Stainless steel	Two steps	Water + Al_2O_3 (47 nm) Water + TiO_2 (47 nm) Water + Cu (47 nm)	Tube: Horizontal cylinder/d_o = 1.3 and 3 mm, L = 180 mm	100 °C/0.01–1% (mass)	↓ ↓ ↓
Kedzierski [163]	HTC	Copper	Obtained from manufacturer and diluted	R134a/Polyolester + Al_2O_3 (10 nm)	Block: Rectangular horizontal flat finned surface/101.6 mm × 25.4 mm, fins: h = 76 μm, w = 36 μm, 826 fins per meter	4.4 °C/1.6–5.1% (vol)	↑ ↓ Ø = 5.1%
Diao et al. [32]	HTC, CHF	–	Two steps + surfactant	R141b + Cu (30 nm)	Block: Square horizontal flat surface/–	31.7 °C/ 0.008–0.05% (vol)	↑

Table 2 (continued)

Authors	Subject of study	Substrate material	Preparation method	Composition	Heater type/Dimensions	T/ϕ	Effect on HTC
Cieslinski and Kaczmarczyk [164]	HTC	Stainless steel smooth	Two steps	Water + Al_2O_3 (47 nm)	Tube: Horizontal cylinder/d_o = 10 mm, L = 100 mm	45.8, 100 and 120 °C/ 0.01–1% (mass)	↓
		Stainless steel covered with aluminum		Water + Cu (48 nm)			↑
Sarafraz and Hormozi [165]	HTC	Stainless steel	Two steps	Water + CuO (50 nm)	Tube: Horizontal cylinder/d_o = 21 mm, L = 350 mm (total), 105 mm (heated)	100 °C/0.1–0.4% (mass)	↓
			Two steps + surfactant				↓
Hu et al. [166]	HTC, CHF	Platinum	Two steps	Water + circular graphene nanosheets (t = 0.335–3.35 nm and d = 10–20 μm)	Horizontal wire/d = 0.07 mm, L = 100 mm	100 °C/ 0.005–0.1% (mass)	↑
Sarafraz et al. [33]	HTC, CHF	Copper	Two steps	Water/Ethylene–glycol + ZrO_2 (20–25 nm)	Block: Circular horizontal flat surface/ d = 11 mm	100 °C/ 0.025–0.1% (mass)	↑
Sarafraz and Hormozi [167]	HTC, CHF	Copper	Two steps + surfactant	Water + CNT (d = 10–20 nm, L = 1.5–2 μm)	Block: Circular horizontal flat surface/ d = 11 mm	100 °C/0.1 and 0.3% (mass)	↓
Sarafraz et al. [168]	HTC, CHF	Copper	Two steps + surfactant	Water + Al_2O_3 (20 nm)	Block: Circular horizontal flat surface/ d = 11 mm	100 °C/0.1–0.3% (mass)	↑
				Water + Al_2O_3 (50 nm)			↓
Ciloglu [169]	HTC, CHF	Copper	Two steps	Water + SiO_2 (414 nm)	Block: Hemispherical surface/d = 40 mm	100 °C/ 0.01–0.1% (vol)	↓
Manetti et al. [170]	HTC	Copper	Two steps	Water + Al_2O_3 (10 nm)	Block: Circular horizontal flat surface/ d = 20 mm	100 °C/0.0007 – 0.007% (vol)	↑ smooth surface
							↓ rough surface
Rainho Neto et al. [34]	HTC, CHF	Copper	Two steps	Water + Al_2O_3 (80 – 100 nm)	Block: Circular horizontal flat surface/ d = 12 mm	100 °C/0.02% (vol)	↓
				Water + Fe_2O_3 (70 – 100 nm)			↓
				Water + CNT (50 – 100 nm)			↔
				Water + CNT (50 – 100 nm)		100 °C/0.1% (vol)	↓

CHF = critical heat flux; ↑ increase; ↓ decrease; ↔ non-noticeable effect; *rough surface; **smooth surface; [+]dimension of the nanoparticles not informed

phase with dimensions varying from 20 to 250 nm, namely alumina, titania, diamond, copper oxide, copper, zinc oxide, and zirconia nanoparticles, carbon nanotubes, and circular graphene nanosheets. Boiling occurred over stainless steel, copper, nickel, nickel + chromium, platinum, and aluminum substrates. Overall, heat transfer behavior could not be correlated to particles dimensions, according to results presented in this table. Also, heat transfer intensification usually happened for nanofluids containing less than 1% in volume of nanoparticles, and non-spherical nanoparticles were responsible for steepest rises in HTC values.

Among the works listed in Table 2, 37% reported that the HTC only decreases with the addition of nanoparticles to base fluids, and 24% documented its reduction, enhancement, or non-noticeable effects, depending on the conditions. Consistent increments in HTC were observed in 33% of the investigations, and 6% of the studies only computed minor variations of the HTC [29, 130, 137]. Surface modifications due to nanoparticles deposition and variations of the transport properties of the fluid were pointed out as probable reasons for the occurrence of both increments and reductions in the HTC [62, 135, 140, 144, 145, 151, 152, 154].

It should be remarked that some authors noticed optima volumetric concentration values, which resulted in maximum values for HTC and CHF [135, 145, 155, 159, 166]. These authors claimed that higher concentrations than the optimum value result in decrement of the number of active bubble nucleation sites, due to intensified deposition of particles on the heated surface. Kwark et al. [121] identified an optimum concentration that promoted increment in CHF with minor deterioration of the HTC. In addition, Chopkar et al. [62] and Kedzierski [163] found highest rises of the HTC for the lowest nanoparticle concentrations evaluated by them, and Duangthongsuk et al. [156] observed lowest decreases in the HTC with less concentrated nanofluids. Rainho Neto et al. [34] obtained similar values of HTC for distilled water and nanofluid containing 0.02% of carbon nanotubes dispersed in water, while the CHF for this nanofluid was enhanced by 29% if compared to pure water. All other nanofluids studied by Rainho Neto et al. [34] presented reductions in the HTC and increases in the CHF, which were mainly attributed to surface wettability modifications and thermal resistance of the deposited porous layer with vapor compartments. Suriyawong and Wongwises [141] detected enhancements in the HTC for nanofluids containing less than 0.0001% in volume of dispersed phase. They claimed that the heat transfer coefficient was enhanced due to thermal conductivity augmentation, and that effects on bubble nucleation caused by particle deposition were negligible at concentrations as low as 0.0001%. In this context, Suriyawong and Wongwises [141] suggested that high volumetric concentrations imply on intensified particle deposition, creating an additional thermal resistance between the heated surface and the fluid, thus diminishing the number of active bubble nucleation sites and deteriorating the HTC.

Various researchers attributed changes in the HTC to the deposition of nanoparticles on the heated surface [33, 136, 139, 142, 144, 150, 153, 155, 156, 159, 160, 164, 165, 169]. Some authors speculate that pool boiling heat transfer of nanofluids is strongly affected by the ratio between original surface roughness and dimensions of dispersed particles [134, 171, 172]. Therefore, for cases in which particles dimensions are comparable to surface roughness, the deposition could fill the original cavities and reduce the number of active bubble nucleation sites and the heat transfer coefficient, while sedimentation of smaller particles could just split the active nucleation sites, thus increasing their number and the effective heat transfer coefficient. Diao et al. [32] considered that the enhancement caused by the existence of more nucleation sites is greater than the deleterious effects of an additional thermal resistance related to the deposited layer, which results in augmentation of the HTC with the use of nanofluids.

As already mentioned, the deposition of nanoparticles on a surface can modify its wettability. Some authors referred to the wettability increment, corresponding to smaller contact angles, to justify reductions in the HTC [31, 139, 168, 171, 173]. Although wettability augmentation may be responsible for reducing the HTC, Liu et al. [145] indicated that the reduction in the contact angle increases the area where the microlayer evaporation occurs during bubble growth. According to these authors, this secondary effect combined with the thermal conductivity increase may enhance the effective HTC of nanofluids compared to the pure base fluids. Sarafraz et al. [168] also observed HTC enhancements with the addition of nanoparticles to a base fluid, which they attributed to rises in thermal conductivity due to nanoparticles mobility and Brownian movements.

According to Sarafraz et al. [33], the increment in the surface roughness and consequently, of the number of active nucleation sites and bubble frequency, is an additional effect associated with the nanoparticles deposition that may also contribute to the heat transfer enhancement. Nevertheless, the deposition of nanoparticles is also indicated as detrimental to the HTC. In fact, a number of authors suggested that an additional thermal resistance is created by nanoparticle deposition, reducing the effective HTC [136, 139, 141, 149, 151, 157, 165, 167, 169]. In a similar trend, authors have pointed out changes in the surface texture as the reasons for the deterioration of the HTC with the addition of nanoparticles to a fluid

[27, 121, 129, 132, 157, 158, 164], but no physical mechanisms were explored or suggested as responsible for their conclusions.

Thermal conductivity augmentation due to the addition of nanoparticles to a base fluid was accounted as the cause for rises in the HTC observed by some authors [131, 133, 147]. Wen and Ding [131] also attributed such rises to modifications of fluid–surface interactions, but no specific mechanism was mentioned, while Heris [147] listed the increase in the number of active bubble nucleation sites and the larger diameter of bubble detachment for a fixed detachment frequency as the additional mechanisms responsible for HTC enhancements noted for nanofluids, if compared to pure base fluids. Overall, the main reasons for variations in HTC values found in the literature are the deposition of nanoparticles onto the heated substrate, which modifies the bubble nucleation process and changes fluids transport properties, especially thermal conductivity.

5.3 Flow boiling of nanofluids

Although there are relatively few studies on flow boiling of nanofluids compared to single-phase flow and pool boiling, this subject has attracted much interest over the last years, especially due to its potential to remove high heat fluxes. Table 3 describes investigations concerning flow boiling of nanofluids. Most flow boiling works were carried out with water-based nanofluids, as observed for single-phase and pool boiling investigations. However, a significant part of studies concerning flow boiling also dealt with R141b-based nanofluids, while some still used R113, R134a, ethanol, or R134a + polyolester, R134a + ester, and R600a + polyolester solutions as base fluids. Dispersed phases composed by nanoparticles with dimensions varying from 13 to 300 nm were evaluated, and the employed materials were Al_2O_3, AlN, SiC, SiO_2, CuO, C-diamond, ZnO, Cu, Ag, and Al. Channels made of stainless steel, copper, Pyrex, and aluminum were employed. In a similar manner to what was observed for pool boiling, no relation could be drawn between particle sizes or material and flow boiling HTC. Also, as was noticed in the analysis of pool boiling investigations, HTC enhancements are more commonly found for nanofluids containing less than 1% in volume of nanoparticles. The effect of nanoparticles geometry on the HTC was investigated only in one study.

About 55% of the studies listed in Table 3 reported only increments on the HTC of nanofluids under flow boiling conditions with the addition of nanoparticles. In 21% of these investigations increase, decrease, or non-noticeable effects on the HTC were noticed, depending on experimental conditions [176, 184, 189, 193, 198, 199]. Some authors observed only reductions in the HTC with the addition of nanoparticles, corresponding to 14% of the listed works [178, 188, 191, 194], while others (7%) did not observe significant HTC variations [28, 32]. Yang and Liu [180] and Dursma et al. [190] recommended 0.003 and 0.05%, respectively, as optimal volumetric concentrations of nanoparticles, to obtain a maximum flow boiling HTC. Finally, Lee and Mudawar [80] verified the blockage of a microchannel with original hydraulic diameter equal to 341 μm due to deposition of nanoparticles, and therefore, they could not evaluate the HTC. The presence of nanoparticles in a base fluid is also responsible for diminishing thermal instabilities, which were evaluated through amplitudes of temperature variation on the heated surface for steady-state conditions [179, 191]. Such behavior was attributed to a reduction in nanofluids surface tension, which is associated with smaller bubble detachment diameters. Yu et al. [191] still mentioned that particles deposition suppresses the number of active bubble nucleation sites, thus reducing thermal instability.

As was observed in studies concerning pool boiling, deposition of nanoparticles on the heated surface was indicated as responsible for changes in HTC by some researchers [178, 186, 188, 196, 199, 200]. Abedini et al. [178] suggested that an increment in surface wettability caused by the deposition of nanoparticles promotes larger bubble detachment diameters, thus reducing bubble detachment frequency and the HTC. Sarafraz and Hormozi [188] speculated that particles deposition reduces the number of active bubble nucleation sites and, consequently, the HTC. In another study, Sarafraz and Hormozi [200] still attributed the diminution of the HTC to increases in surface wettability and to the additional thermal resistance of the deposited layer.

Henderson et al. [176] claimed that the decrease in the HTC is likely owed to difficulties in obtaining stable nanofluids. However, it should be remarked that these authors conducted experiments for reduced vapor qualities, up to 0.2; thus, the reduction observed by Henderson et al. [176] could also be related to the suppression of bubble nucleation caused by particles deposition, as reported by Cieslinski and Kaczmarczyk [164] for pool boiling of nanofluids. Some works also attributed the enhancement of the HTC to surface modifications, but no further discussion on the physical mechanisms was given [186, 196]. Moreira et al. [199] performed a surface analysis for a bare microtube and for the same tube with deposited nanoparticles, comparing the diameter of the existent cavities on the surface with the model of Kandlikar et al. [201] for the onset of nucleate boiling under conditions of convective boiling inside microchannels. As a result, no meaningful difference between the number of cavities on the active range for bubble nucleation was observed for surfaces covered by nanoparticles larger than 40 nm and the as-received channel. However, in

Table 3 Summary of experimental conditions and results for investigations concerning flow boiling of nanofluids

Authors	Subject of study/channel material	Preparation method	Composition	q [kW/m^2]/G [kg/m^{2}s]/d_h [mm]	T/ϕ	Effect on HTC
Faulkner et al. [28]	HTC/–	Two steps + surfactant	Water + Al-N* Water + Al_2O_3* Water + SiC*	2750/266–532/0.96	100 °C/0.25–0.5% (mass)	↔
Lee and Mudawar [80]	HTC/copper	Obtained from manufacturer and diluted	Water + Al_2O_3 (36 nm)	–/–/0.341	–	Blockage of the channel and CHF
Bartelt et al. [174]	HTC/copper	Obtained from manufacturer and diluted	R134a/Polyoles-ter + CuO (30 nm)	0.69–3.06/125–390/7.9	3.6–41 °C/0.5–2% (mass)	↑
Peng et al. [175]	HTC/copper	Two steps	R113 + CuO (40 nm)	3.08–6.16/100–200/8.12	40 °C/0–0.5% (mass)	↑
Henderson et al. [176]	HTC/copper	Obtained from manufacturer and diluted	R134a + SiO_2 (200–300 nm)	5.82–16.17/137–385/7.9	33–38.3 °C/0.05 and 0.5% (vol)	↓
			R134a + Polyoles-ter + CuO (30 nm)	0.69–3.06/125–390/7.9	3.6–41 °C/0.02–0.08% (vol)	↑
Kim et al. [31]	HTC, CHF/stainless steel	Obtained from manufacturer and diluted	Water + Al_2O_3 (40 nm) Water + diamond (165.4 nm) Water + ZnO (77.4 nm)	0–7500/1500–2500/5.53	100 °C/0.001–0.1% (vol)	↔
Boudouh et al. [177]	HTC/copper	Two steps	Water + Cu (35 nm)	–/217–516/0.8	100 °C/5–50 mg/l	↑
Abedini et al. [178]	HTC/stainless steel	Two steps	Water + TiO_2 (20 nm)	51.5–102/137–303/10	90 °C/0.1–2.5% (vol)	↓
Xu and Xu [179]	HTC/Pyrex	Two steps	Water + Al_2O_3 (40 nm)	0–10^4/171.9–401/0.143	100 °C/0.2% (mass)	↑
Yang and Liu [180]	HTC, CHF/copper	Two steps	Water + CuO (50 nm)	1–24/–/8.825	40–70 °C/0.1–1.5% (mass)	↑
Mahbubul et al. [181]	HTC/–	Two steps	R141b + Al_2O_3 (13 nm)	5/100/6	25 °C/1–5% (vol)	↑
Chehade et al. [182]	HTC/copper	Two steps	Water + Ag (35 nm)	–/87–653/0.8	60 °C/0.000237 and 0.000475% (vol)	↑
Rana et al. [183]	Bubble nucleation and growth/stainless steel	Two steps	Water + ZnO (40 nm)	100–450/338.7–680.2/9.1	100 °C/0.0001–0.01% (vol)	↑
Diao et al. [184]	HTC/stainless steel	Two steps + surfactant	R141b + Al_2O_3 (13 nm)	50–800/–/0.4	27.5– 52.9 °C/0.001–0.1% (vol)	↓ ϕ = 0.1% any pressure ↔ ϕ = 0.01 and 0.001% and P > 100 kPa ↑ ϕ = 0.01 and 0.001% 86 > P > 96 kPa
Akhavan-Behabadi et al. [185]	HTC/copper	Two steps	R600a/Polyoles-ter + CuO (50 nm)	3–8/50–400/8.26	29.6–44.7 °C/0.5–1.5% (mass)	↑

Table 3 (continued)

Authors	Subject of study/channel material	Preparation method	Composition	q [kW/m^2]/G [kg/m^{2}s]/d_h [mm]	T/ϕ	Effect on HTC
Rana et al. [186]	Void fraction/stainless steel	Two steps	Water + ZnO (40 nm)	100–550/338.7–680.2/9.1	100 °C/0.001–0.01% (vol)	↑
Sun and Yang [187]	HTC/copper	Two steps + surfactant	R141b + Cu (40 nm)	–/120–330/10	31.7 °C/0.014–0.041 (vol)	↑
			R141b + Al (40 nm)		31.7 °C/0.046–0.137 (vol)	↑
			R141b + Al_2O_3 (40 nm)		31.7 °C/0.031–0.094 (vol)	↑
			R141b + CuO (40 nm)		31.7 °C/0.02–0.06 (vol)	↑
Sarafraz and Hormozi [188]	HTC/stainless steel	Two steps	Water + CuO (50 nm)	8–190/300–1200/30	100 °C/0.5–1.5% (vol)	↓
			Water/Ethylene–glycol + CuO (50 nm)		100 °C/0.1–0.4% (vol)	↓
Sarafraz and Hormozi [189]	HTC/stainless steel	Two steps	Water + Al_2O_3 (50 nm)	8–190/353–1059/30	100 °C/0.5–1.5% (vol)	↑ lower q ↓ higher q
Duursma et al. [190]	HTC/Pyrex	Two steps	Ethanol + Al_2O_3 (50 nm)	1.5–9/11.2–44.8/0.571–1.454	80 °C/0.01–0.1% (vol)	↑
Yu et al. [191]	HTC and thermal instability/stainless steel	Two steps	Water + Al_2O_3*	20–406/680–3100/1.09	118.6 °C/0.01 and 0.1% (vol)	↓
Setoodeh et al. [192]	HTC/Aluminum	Two steps + surfactant	Water + Al_2O_3 (20–30 nm)	200–6000/480–860/24	104.8 °C/0.25% (vol)	↑
Nikkhah et al. [193]	HTC/stainless steel	Two steps + variation of the pH	Water + CuO (50 nm)	0–175/350–1060/30	100 °C/0.1–0.4% (mass)	↑ lower q ↓ higher q
Rajabnia et al. [194]	HTC/stainless steel	Two steps	Water + TiO_2 (20 nm)	38.8–111.46/138–308/10	100 °C/0.01–0.5% (vol)	↓
Wang and Hu [195]	HTC/stainless steel	Two steps	Water + Al_2O_3 (20 nm)	50–300/350–1100/6	120.2–170.4 °C/0.1 and 0.5% (vol)	↑
Tazarv et al. [196]	HTC/–	Two steps + surfactant	R141b + TiO_2 (30 nm)	1.741–27.859/192.5–481.4/8.825	51–58 °C/0.01 and 0.03% (vol)	↑
Sarafraz and Hormozi [197]	HTC/stainless steel	Two steps + surfactant	Water + CuO (45–50 nm)	2.3–210.1/100–1200/30	100 °C/0.1–0.3% (vol)	↑
			Water + Al_2O_3 (50 nm)			↑
			Water + CNT (d = 12–14 nm and L = 1.5–2 μm)			↑
Karimzadehkhouei et al. [198]	HTC/stainless steel	Two steps	Water + Al_2O_3 (20 nm)	–/1200–3400/0.502	–/0.05–1.5% (mass)	↔ low ϕ ↓ high ϕ

Table 3 (continued)

Authors	Subject of study/channel material	Preparation method	Composition	q [kW/m^2]/G [kg/m^{2}s]/d_h [mm]	T/ϕ	Effect on HTC
Moreira et al. [199]	HTC/stainless steel	Two steps	Water + Al_2O_3 (20–30 nm)	100–350/200–600/1.1	102 °C/0.001–0.1% (vol)	↓
			Water + Al_2O_3 (40–80 nm)			↔
			Water + SiO_2 (15 nm)			↓
			Water + SiO_2 (80 nm)			↔ and ↑
			Water + Cu (25 nm)			↓

CHF = critical heat flux; ↑ increase; ↓ decrease; ↔ non-noticeable effect; *dimension of nanoparticles not informed

comparison with the bare tube, surfaces covered by nanoparticles smaller than 30 nm presented a decrease in the number of cavities with diameters within the range of active bubble nucleation. Thus, Moreira et al. [199] indicated that the effect of nanoparticles on the HTC depends on the original texture of the surface and on the size of the nanoparticles, as already pointed out for pool boiling heat transfer. Therefore, the deposition may imply in either increasing or decreasing of the number of active bubble nucleation sites and, consequently, on the same behavior for the HTC.

Some researchers investigated flow boiling of pure base fluids in channels with the surface previously covered by nanoparticles through a boiling process of nanofluids [180, 184, 199]. These investigations focused on segregating effects of surface modification from those associated with the solution itself, related to the addition of nanoparticles to the base fluid. Yang and Liu [180] and Diao et al. [184] observed that the flow boiling HTC of the pure fluid on nanoparticles-coated channels was higher than on bare surfaces. They also pointed out higher HTC values for flow boiling of the base fluid in the tube as commercially available than for flow boiling of the nanofluids in the same tube. Yang and Liu [180] recognized that nanoparticles deposition generates an additional thermal resistance that is detrimental to the effective HTC. This effect was also acknowledged by Sarafaz and Hormozi [197], who stated that highly conducting dispersed phases should be employed, thus resulting in minimum thermal resistance. Moreira et al. [199] verified no influence of the deposition on the HTC for nanoparticles larger than 40 nm, and a reduction in the HTC for nanoparticles smaller than 30 nm, corroborating their conclusions based on the number of cavities on the active range for bubble nucleation, as expressed above. A simple theoretical analysis on the effect of the additional thermal resistance created by the deposited nanoparticles layer on the effective HTC was also carried out by Moreira et al. [199]. From this analysis, they noticed that the effects of the additional thermal resistance resultant from particle deposition are not enough to explain the deterioration of the HTC when observed, because in general the effect of this layer on the HTC is smaller than the usual experimental uncertainties of the HTC estimates. Investigations of flow boiling of R141b and water on surfaces coated by nanoparticles were, respectively, conducted by Diao et al. [184] and Moreira et al. [199]. These authors verified minor variations in the HTC, as can be seen in Fig. 6, corroborating the insignificance of the additional thermal resistance.

Some authors suggested that nanoparticles could have a molecular interfacial layer on their surfaces disturbing the flow, thus causing a reduction in the boundary layer thickness that could be responsible for increasing the HTC

[17, 175, 181, 185]. Boudouh et al. [177] indicated that nanofluids are stirred by bubble growth and detachment, which foments nanoparticles motion and intensify the heat transfer. These authors also stated that increments in the HTC of nanofluids are enhanced with increasing mass velocities, because smaller bubbles are detached from the wall due to the augmentation of drag effect, increasing bubble detachment frequency and inducing nanoparticles motion.

According to the results of Sarafraz and Hormozi [189], which were corroborated by the data of Nikkhah et al. [193] and Rajabnia et al. [194], under conditions prevailing convective effects, the HTC is enhanced with the addition of nanoparticles to a base fluid due to the thermal conductivity augmentation. However, under conditions prevailing nucleate boiling effects, the addition of nanoparticles deteriorates the HTC due to the reduction in the density of active bubble nucleation sites associated with the nanoparticle deposition. In some investigations, increments of the HTC were related to variations of transport properties of nanofluids in comparison with base fluids, especially thermal conductivity and surface tension [180, 187, 195, 197]. Rana et al. [183] and Akhavan-Behabadi et al. [185] suggested that the HTC is higher for a nanofluid than for its base fluid due to the augmentation of the thermal conductivity promoted by the addition of nanoparticles, similarly to what is observed for pool boiling. In contrast, Bartelt et al. [174] stated that thermal conductivity intensification alone cannot explain the augmentations of up to 101% in the HTC they have obtained.

Yu et al. [191] verified that the addition of nanoparticles to a base fluid promotes reductions in the HTC and thermal instability effects, while Xu and Xu [179] associated HTC magnifications to the reduction in thermal instabilities, with suppression of intermittent dry-outs related to flow oscillations due to thermal instabilities. For elongated bubbles and annular flow patterns in microchannels, Xu and Xu [179] pointed out the increment in the thermal conductivity of the liquid film associated with the local augmentation of the particle concentration due to the evaporation of the base fluid as the factor responsible for increasing the HTC.

Figure 7 depicts the effects of the variation of the nanoparticles concentration on the HTC due to the evaporation process according to the correlation proposed by Liu and Winterton [202] for fluids without particles, which is given by the asymptotic sum of nucleate boiling and convective effects, allowing the evaluation of each parcel individually. Figure 7 also shows the evaluation of the nanoparticle volumetric concentration along the evaporation process. In this figure, a dispersion of copper nanoparticles in water was considered, and the thermal conductivity of the nanofluid was estimated according to Nan et al. [70], the dynamic viscosity according to Einstein's model [78], and the density was calculated based on the classical rule of mixtures. HTC results are displayed in Fig. 7 for inlet nanoparticle volumetric concentrations of

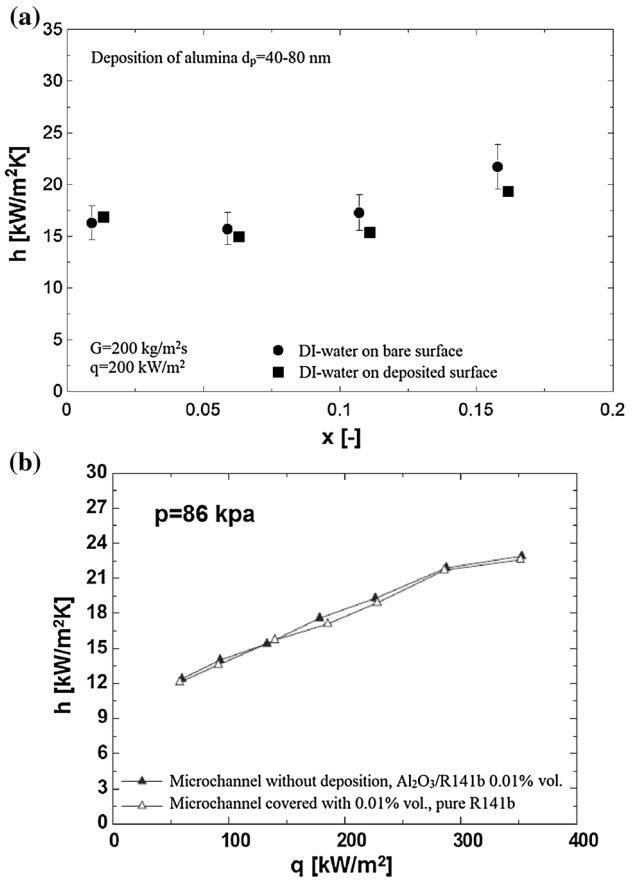

Fig. 6 Effect of nanoparticle deposition on the HTC. **a** Diao et al. [184]; **b** Moreira et al. [199]

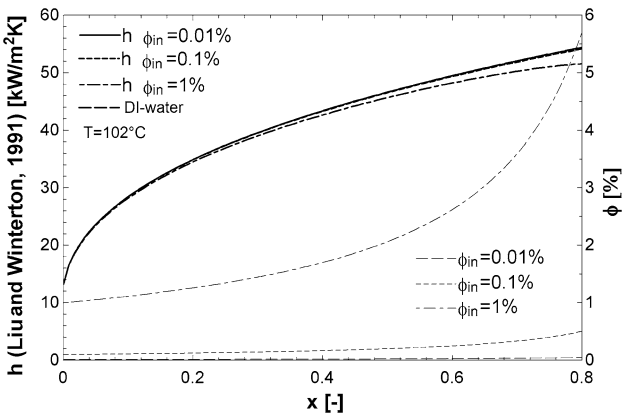

Fig. 7 Effects of vapor quality in the flow boiling HTC of copper + water nanofluids and on the volumetric concentration of nanoparticles in the liquid phase

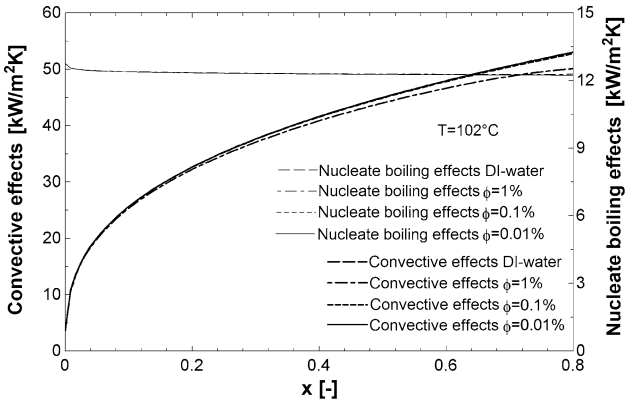

Fig. 8 Effects of vapor quality variation in convective and nucleated boiling according to Liu and Winterton [202]

0.01, 0.1, and 1%. The HTC was calculated up to a maximum vapor quality of 0.8, because wall dry-out is expected under conditions of higher vapor quality. According to Fig. 7, the nanoparticle volumetric concentration of the liquid phase presents an exponential behavior with increasing the vapor quality. Moreover, as shown in this figure and contrarily to the hypothesis of Xu and Xu [179], the HTC decreases with increasing ϕ at high vapor quality conditions, even though the nanoparticles concentration in the liquid and, consequently, its thermal conductivity grow. It is important to highlight that such an analysis takes into account only the effect on the liquid properties of adding nanoparticles to a base fluid, neglecting effects associated with modifications of the surface texture, once that the Liu and Winterton [202] predictive method takes into account for the nucleate boiling the Cooper [203] correlation, which does not consider surface tension and texture effects, except by the surface roughness.

Figure 8 displays the variation with vapor quality of the contributions to the HTC of nucleate boiling and convective effects according to the Liu and Winterton [202] model, considering the same conditions in Fig. 7. The contribution of nucleate boiling effect is given as the product of the pool boiling HTC and the nucleate boiling suppression factor, while the contribution of convective effects consists of the product of the single-phase forced convection HTC and the convective enhancement factor. Figure 8 shows that nucleated boiling presents negligible sensitivity to variations in nanofluids concentration, while convective boiling is significantly reduced for higher concentrations. As the dynamic viscosity increases with nanoparticles concentration, the Reynolds number of the liquid phase drops, increasing the liquid film thickness, and

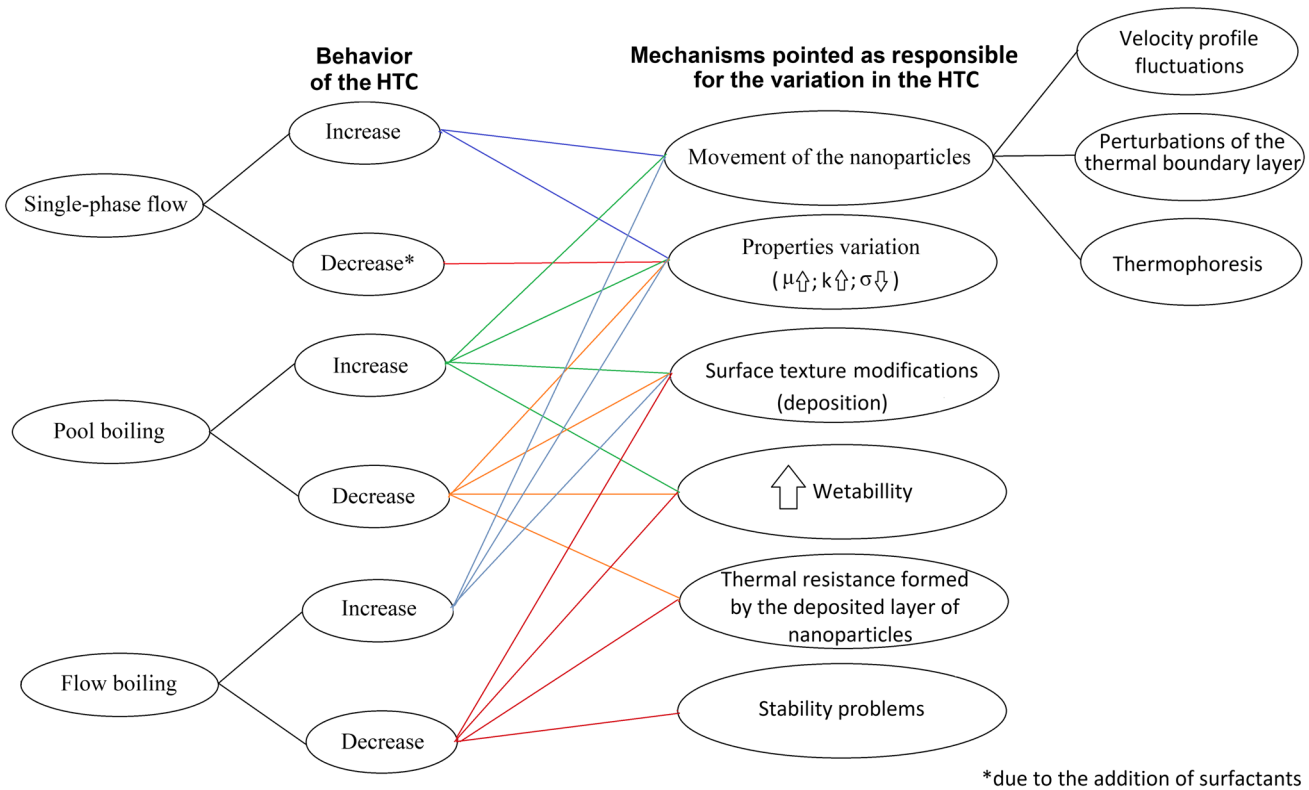

Fig. 9 Schematic diagram of physical mechanisms related to observed variations of the HTC due to the addition of nanoparticles to base fluids, according to the literature

this effect overlaps the intensification of the HTC promoted by thermal conductivity augmentation. It should be remarked, however, that variations of the HTC are noticed for concentrations higher than 1%, and usually the employed nanofluids have low volumetric concentrations, commonly around 0.1%, but ranging from 0.00001% to 2.5%, as seen in Table 3.

6 Conclusions

This work presented a broad literature review concerning nanofluids applied as heat transfer fluids. Based on the present analysis, it is evident that most works are focused on single-phase flows and pool boiling, while fewer studies involving flow boiling can also be found. A variety of physical mechanisms are pointed out by distinct authors as responsible for heat transfer intensification or deterioration obtained with the use of nanofluids compared to their base fluids performance. Figure 9 summarizes these physical mechanisms in a diagram and shows the corresponding effects observed for single-phase flow, pool boiling and flow boiling.

In general, the HTC of single-phase flow rises with the addition of nanoparticles to a fluid, which was explained by most authors as a result of thermal conductivity augmentation and also due to nanoparticles motion. For laminar flows, maxima values of HTC increments were observed in the thermal developing region. The main plausible reasons indicated by the authors as the effects of adding nanoparticles to a base fluid in pool boiling HTC were: changes in the fluid transport properties, especially thermal conductivity and surface tension; and modifications in the texture of heated surfaces caused by nanoparticles deposition, affecting the number of active bubble nucleation sites. Investigations concerning flow boiling converge to similar mechanisms to those noticed for pool boiling, i.e., variation of transport properties and surface characteristics. Usually, augmentations in thermal conductivity were related to an increase in the HTC for convective dominated flow boiling, while for nucleated boiling the changes in heat transfer behavior are related to variations in surface texture. It is worth noting that the addition of nanoparticles also resulted in reduction in thermal instabilities, justified by a decrease in the number of active bubble nucleation sites and surface tension observed for nanofluids compared to the base fluid. As a final comment, it should be remarked that even though many authors indicate that particle deposition affects the number of active bubble nucleation sites, there is a lack of detailed analysis regarding surface textures prior and after boiling and bubble nucleation criteria.

Acknowledgements The authors gratefully acknowledge the financial support provided by CAPES (Coordination for the Improvement of Higher Level Personal, Brazil) through the NANOBIOTEC research program, CNPq (National Council for Scientific and Technological Development, Brazil) under Contract Numbers 303852/2013-5, 404437/2015-0 and 131082/2015-9. The authors also acknowledge the FAPESP (São Paulo State Research Foundation, Brazil) for the scholarships under Contract Numbers 2016/16849-3, and 2015/24834-3 and the research Grant 2016/09509-1.

References

1. Pop E (2010) Energy dissipation and transport in nanoscale devices. Nano Res 3(3):147–169
2. Li Z, Kandlikar SG (2015) Current status and future trends in data-center cooling technologies. Heat Transf Eng 36:523–538
3. Agostini B, Fabbri M, Park JE, Wojtan L, Thome JR, Michel B (2007) State of the art of high heat flux cooling technologies. Heat Transf Eng 22(4):258–281
4. Jakhar S, Sonni MS, Gakkhar N (2016) Historical and recent development of concentrating photovoltaic cooling technologies. Renew Sustain Energy Rev 60:41–59
5. Zimmermann S, Meijer I, Tiwari MK, Paredes S, Michel B, Poulikakos D (2012) Aquasar: a hot water cooled data center with direct energy reuse. Energy 43:237–245
6. Zimmermann S, Helmers H, Tiwari MK, Paredes S, Michel B, Wiesenfarth M, Bett AW, Poulikakos D (2015) A high-efficiency hybrid high-concentration photovoltaic system. Int J Heat Mass Transf 89:514–521
7. Kandlikar SG (2016) Mechanistic considerations for enhancing flow boiling heat transfer in microchannels. J Heat Transf 138:021504
8. Choi SUS, Eastman JA (1995) Enhancing thermal conductivity of fluids with nanoparticles. No. ANL/MSD/CP-84938; CONF–951135—29. Argonne National Lab., IL
9. Babita Sharma SK, Gupta SM (2016) Preparation and evaluation of stable nanofluids for heat transfer application: a review. Exp Therm Fluid Sci 79:202–212
10. Lomascolo M, Colangelo G, Milanese M, Risi A (2015) Review of heat transfer in nanofluids: conductive, convective and radiative experimental results. Renew Sustain Energy Rev 43:1182–1198
11. Yang Y, Zhang ZG, Grulke EA, Anderson WB, Wu G (2005) Heat transfer properties of nanoparticle-in-fluid dispersions (nanofluids) in laminar flows. Int J Heat Mass Transf 48:1107–1116
12. Masuda H, Ebata A, Teramae K, Hishinima N (1993) Alteration of thermal conductivity and viscosity of liquid by dispersing ultrafine particles (dispersion of Al_2O_3, SiO_2 and TiO_2 ultrafine particles). Netsu Bussei 4(4):227–233
13. Angayarkanni SA, Philip J (2015) Review on thermal properties of nanofluids: recent developments. Adv Coll Interface Sci 225:146–176
14. Kakaç S, Pramuanjaroenkij A (2016) Single-phase and two-phase treatments of convective heat transfer enhancement with nanofluids—a state-of-the-art review. Int J Therm Sci 100:75–97
15. Ciloglu D, Blukbasi A (2015) A comprehensive review on pool boiling of nanofluids. Appl Therm Eng 84:45–63
16. Fang X, Wang R, Chen W, Zhang H, Ma C (2015) A review on flow boiling heat transfer of nanofluids. Appl Therm Eng 91:1003–1017
17. Pinto RV, Fiorelli FAS (2016) Review of the mechanisms responsible for heat transfer enhancement using nanofluids. Appl Therm Eng 108:720–739

18. Fang X, Chen Y, Zhang H, Chen W, Dong A, Wang R (2016) Heat transfer and critical heat flux of nanofluid boiling: a comprehensive review. Renew Sustain Energy Rev 62:924–940
19. Pak BC, Cho YI (1998) Hydrodynamic and heat transfer study of dispersed fluids with submicron metallic oxide particles. Exp Heat Transf 11:151–170
20. Lee S, Choi SUS, Li S, Eastman JA (1999) Measuring thermal conductivity of fluids containing oxide nanoparticles. J Heat Transf 121:280–289
21. Hamilton RL, Crosser OK (1962) Thermal conductivity of heterogeneous two-component systems. Ind Eng Chem Fundam 1(3):187–191
22. Xuan Y, Li Q (2000) Heat transfer enhancement of nanofluids. Int J Heat Fluid Flow 21:58–64
23. Li CH, Paterson GP (2006) Experimental investigation of temperature and volume fraction variations on the effective thermal conductivity of nanoparticle suspensions (nanofluids). J Appl Phys 99:084314
24. Das SK, Putra N, Thiesen P, Roetzel W (2003) Temperature dependence of thermal conductivity enhancement for nanofluids. J Heat Transf 125:567–574
25. Buongiorno J, Venerus DC, Prabhat N, Mckrell L, Townsend J, Christianson R, Tolmachev YV, Keblinski P, Hu L, Alvarado JL, Bang IC, Bishnoi SW, Bonetti M, Botz F, Cecere A, Chang Y, Chen G, Chen H, Chung SJ, Chyu MK, Das SK, Di Paola R, Ding Y, Dubois F, Dzido G, Eapen J, Escher W, Funfschilling D, Galand Q, Gao J, Gharagozloo PE, Goodson KE, Gutierrez JG, Hong H, Horton M, Hwang KS, Iorio CS, Jang SP, Jarzebski AB, Jiang Y, Jin L, Kabelac S, Kamath A, Kedzierski MA, Kieng LG, Kim C, Kim J-H, Kim S, Lee SH, Leong KC, Manna I, Michel B, Ni R, Patel HE, Philip J, Poulikakos D, Reynaud C, Savino R, Singh PK, Song P, Sundararajan T, Timofeeva E, Tritcak T, Turanov AN, Van Vaerenbergh S, Wen D, Witharana S, Yang C, Yeh W-H, Zhao X-Z, Zhou S-Q (2009) A benchmark study on the thermal conductivity of nanofluids. J Appl Phys 106:094312
26. Tertsidou GJ, Tsolakidou CM, Pantzali M, Assael MJ, Colla L, Fedele L, Bobbo S, Wakeham WA (2016) New measurements of the apparent thermal conductivity of nanofluids and investigation of their heat transfer capabilities. J Chem Eng Data 62:491–507
27. Das SK, Putra N, Roetzel W (2003) Pool boiling characteristics of nano-fluids. Int J Heat Mass Transf 46:851–862
28. Faulkner D, Khotan M, Sherrakiz R (2003) Practical design of a 1000 W/cm(2) cooling system. In: 19th Annual symposium semiconductor thermal measurement and management symposium, Fairmont, EUA
29. You SM, Kim JH, Kim KH (2003) Effect of nanoparticles on critical heat flux of water in pool boiling heat transfer. Appl Phys Lett 83:3374–3376
30. Buongiorno J (2013) Can corrosion and CRUD actually improve safety margins in nuclear plants? In: 8th International conference on multiphase flow, Jeju, South Korea
31. Kim SJ, McKrell T, Buongiorno J, Hu LW (2010) Subcooled flow boiling heat transfer of dilute alumina, zinc oxide, and diamond nanofluids at atmospheric pressure. Nucl Eng Des 240:1186–1194
32. Diao YH, Li CZ, Zhao YH, Liu Y, Wang S (2015) Experimental investigation on the pool boiling characteristics and critical heat flux of Cu-R141b nanorefrigerant under atmospheric pressure. Int J Heat Mass Transf 89:110–115
33. Sarafraz MM, Kiani T, Hormozi F (2016) Critical heat flux and pool boiling heat transfer analysis of synthesized zirconia aqueous nano-fluids. Int Commun Heat Mass Transf 70:75–83
34. Rainho Neto A, Oliveira JLG, Passos JC (2017) Heat transfer coefficient and critical heat flux during nucleate pool boiling of water in the presence of nanoparticles of alumina, maghemite and CNTs. Appl Therm Eng 111:1493–1506
35. Das KS, Choi SUS, Yu W, Pradeep T (2007) Nanofluids, science and technology. Wiley-Interscience, New York
36. Ghadimi A, Saidur R, Metselaar HSC (2011) A review of nanofluid stability properties and characterization in stationary conditions. Int J Heat Mass Transf 54:4051–4068
37. Wu D, Zhu H, Wang L, Liua L (2009) Critical issues in nanofluids preparation, characterization and thermal conductivity. Curr Nanosci 5:103–112
38. Moraes AAU (2012) Avaliação teórica e experimental do coeficiente de transferência de calor e fluxo crítico durante a ebulição convectiva de nanofluidos. Post-doctoral report, CAPES-NANOBIOTEC
39. Hwang Y, Lee JK, Lee CH, Jung YM, Cheong SI, Lee CG, Ku BC, Jang SP (2007) Stability and thermal conductivity characteristics of nanofluids. Thermochim Acta 455(1–2):70–74
40. Jin H, Xianju W, Qiong L, Xueyi W, Yunjin Z, Liming L (2009) Influence of pH on the stability characteristics of nanofluids. In: Symposium on photonics and optoelectronics, Wuhan, China
41. Lee D, Kim W, Kim BG (2006) A new parameter to control heat transport in nanofluids: surface charge of the particle in suspension. J Phys Chem B 110(9):4323–4328
42. Huang J, Wang X (2009) Influence of pH on the stability characteristics of nanofluid. In: Symposium on photonics and optoelectronics, Wuhan, China
43. Zhu D, Li X, Wang N, Wang X, Gao J, Li H (2009) Dispersion behavior and thermal conductivity characteristics of Al_2O_3-H_2O nanofluids. Curr Appl Phys 9:131–139
44. Beck MP, Yuan Y, Warrier P, Teja AS (2009) The effect of nanoparticle size on the thermal conductivity of alumina nanofluids. J Nanopart Res 11(5):1126–1136
45. Oliveira LR, Silva ACA, Dantas NO, Bandarra Filho EP (2017) Thermophysical properties of TiO_2-PVA/water nanofluids. Int J Heat Mass Transf 115:795–808
46. Zhang H, Shao S, Xu H, Tian C (2013) Heat transfer and flow features of Al_2O_3-water nanofluids flowing through a circular microchannel—experimental results and correlations. Appl Therm Eng 61:86–92
47. Esfahani JA, Safaei MR, Goharimanesh M, Oliveira LR, Goodarzi M, Shamshirband S, Bandarra Filho EP (2017) Comparison of experimental data, modeling and non-linear regression on transport properties of mineral oil based nanofluids. Powder Technol 317:458–470
48. Keblinski P, Phillpot SR, Choi SUS, Eastman JA (2002) Mechanisms of heat flow in suspensions of nano-sized particles (nanofluids). Int J Heat Mass Transf 45:855–863
49. Choi SUS, Zhang ZG, Yu W, Lockwood FE, Grulke EA (2001) Anomalous thermal conductivity enhancement in nanotube suspensions. Appl Phys Lett 79(14):2252–2254
50. Trisaksri V, Wongwises S (2007) Critical review of heat transfer characteristics of the nanofluids. Renew Sustain Energy Rev 11:512–523
51. Wang X, Mujumdar AS (2007) Heat transfer characteristics of nanofluids: a review. Int J Therm Sci 46(1):1–19
52. Paul G, Chopkar M, Manna L, Das PK (2010) Techniques for measuring the thermal conductivity of nanofluids: a review. Renew Sustain Energy Rev 14(7):1913–1924
53. Murshed SMS, Leong KC, Yang C (2008) Investigation of thermal conductivity and viscosity of nanofluids. Int J Therm Sci 47:560–568
54. Xie H, Wang J, Xi T, Liu Y (2002) Thermal conductivity of suspensions containing nanosized SiC particles. Int J Thermophys 23(2):571–580

55. Li Q, Xuan Y, Wang J (2003) Investigation on convective heat transfer and flow features of nanofluids. J Heat Transf 125:151–155
56. Hong TK, Yang HS, Choi CJ (2005) Study of the enhanced thermal conductivity of Fe nanofluids. J Appl Phys 97:064311
57. Motta FC (2011) Caracterização de propriedades termodinâmicas e de transporte de nanofluidos. Master thesis. University of São Paulo
58. Barbes V, Paramo R, Blanco E, Pastoriza-Gallego MJ, Piñeiro MM, Legido JL, Casanova C (2013) Thermal conductivity and specific heat capacity measurements of Al_2O_3 nanofluids. J Therm Anal Calorim 111:1615–1625
59. Fontes DH, Ribatski G, Bandarra Filho EP (2015) Experimental evaluation of thermal conductivity, viscosity and breakdown voltage AC of carbon nanotubes and diamond in transformer oil. Diam Relat Mater 58:115–121
60. Murshed SMS, Leong KC, Yang C (2005) Enhanced thermal conductivity of TiO_2-water based nanofluids. Int J Therm Sci 44(4):367–373
61. Feng Y, Yu B, Xu P, Zou M (2007) The effective thermal conductivity of nanofluids based on the nanolayer and the aggregation of nanoparticles. J Phys D Appl Phys 40(10):3164–3171
62. Chopkar M, Das AK, Manna L, Das PK (2008) Pool boiling heat transfer characteristics of ZrO_2-water based nanofluids from a flat surface in a pool. Heat Mass Transf 44(8):999–1004
63. Colangelo G, Favale E, De Risi A, Laforgia D (2012) Results of experimental investigations on the heat conductivity of nanofluids based on diathermic oil for high temperature applications. Appl Energy 97:828–833
64. Mintsa HA, Roy G, Nguyen CT, Doucet D (2009) New temperature dependent thermal conductivity data for water-based nanofluids. Int J Therm Sci 48(2):363–371
65. Li CH, Willians W, Buongiorno J, Hu LW, Peterson GP (2008) Transient and steady-state experimental comparison study of effective thermal conductivity of Al_2O_3/water nanofluids. J Heat Transf 130(4):042407
66. Ding Y, Alias H, Wen D, Williams RA (2006) Heat transfer of aqueous suspensions of carbon nanotubes (CNT nanofluids). Int J Heat Mass Transf 49:240–250
67. Yamsawasd T, Dalkilic AS, Wongwises S (2012) Measurement of the thermal conductivity of titania and alumina nanofluids. Thermochim Acta 545:48–56
68. Turgut A, Tavman I, Chirtoc M, Schuchmann HP, Sauter C, Tavaman S (2009) Thermal conductivity and viscosity measurements of water-based TiO_2 nanofluids. Int J Thermophys 30:1213–1226
69. Maxwell JC (1873) A treatise on electricity and magnetism, vol I. Clarenton Press, Oxford
70. Nan C-W, Birringer R, Clarke DR, Gleiter H (1997) Effective of particulate composites with interfacial thermal resistance. J Appl Phys 81:6692–6699
71. Duangthongsuk W, Wongwises S (2009) Heat transfer enhancement and pressure drop characteristics of TiO_2-water nanofluid in a double-tube counter flow heat exchanger. Int J Heat Mass Transf 52:2059–2067
72. Akhavan-Zanjani H, Saffar-Avval M, Mansourkiaei M, Sharif F, Ahadi M (2016) Experimental investigation of laminar forced convective heat transfer of Graphene-water nanofluid inside circular tube. Int J Therm Sci 100:316–323
73. White FM (2006) Viscous fluid flow, 3rd edn. McGraw Hill, New York
74. Mena JB, Moraes AAU, Benito YR, Ribatski G, Parise JAR (2013) Extrapolation of Al_2O_3-water nanofluid viscosity for temperatures and volume concentrations beyond the range of validity of existing correlations. Appl Therm Eng 51:1092–1097
75. Wang X, Xu X, Choi SUS (1999) Thermal conductivity of nanoparticle-fluid mixture. J Thermophys Heat Transf 13:474–480
76. Nguyen CT, Desgranges F, Galanis N, Roy G, Maré T, Boucher S, Mintsa HA (2008) Viscosity data for Al_2O_3-water nanofluid-hysteresis: is heat transfer enhancement using nanofluids reliable? Int J Therm Sci 42(2):103–111
77. Timofeeva EV, Routbourt JL, Singh D (2009) Particle shape effects on thermophysical properties of alumina nanofluids. J Appl Phys 106(1):014304
78. Einstein A (1906) Eine neue bestimmung der moleküldimensionen. Ann Phys 324(2):289–306
79. Wen D, Ding Y (2006) Natural convective heat transfer of suspensions of titanium dioxide nanoparticles (Nanofluids). IEEE Trans Nanotechnol 5:220–226
80. Lee J, Mudawar I (2007) Assessment of the effectiveness of nanofluids for single-phase and two-phase heat transfer in micro-channels. Int J Heat Mass Transf 50:452–463
81. Brinkman HC (1952) The viscosity of concentrated suspensions and solutions. J Chem Phys 20(4):571–571
82. Lundgren TS (1972) Slow flow through stationary random beds and suspensions of spheres. J Fluid Mech 51(2):273–299
83. Graham AL (1981) On the viscosity of suspensions of solid spheres. Appl Sci Res 37(3):275–286
84. Frankel NA, Acrivos A (1967) On the viscosity of concentrated suspensions of solid spheres. Chem Eng Sci 22(6):847–853
85. Godson L, Raja B, Lal DM, Wongwises S (2012) Convective heat transfer characteristics of silver-water nanofluid under laminar and turbulent flow conditions. J Therm Sci Eng Appl 4:031001
86. Li Q, Xuan Y (2002) Convective heat transfer and flow characteristics of Cu-water nanofluid. Sci China Ser E: Technol Sci 45(4):408–416
87. Xuan Y, Li Q (2003) Investigation on convective heat transfer and flow features of nanofluids. J Heat Transf 125:151–155
88. Wen D, Ding Y (2004) Experimental investigation into convective heat transfer of nanofluids at the entrance region under laminar flow conditions. Int J Heat Mass Transf 47:5181–5188
89. Heris SZ, Etemad G, Esfahany MN (2006) Experimental investigation of oxide nanofluids laminar flow convection heat transfer. Int Commun Heat Mass Transf 33:529–535
90. He Y, Jin Y, Chen H, Ding Y, Cang D, Lu H (2007) Heat transfer and flow behaviour of aqueous suspensions of TiO_2 nanoparticles (nanofluids) flowing upward through a vertical pipe. Int J Heat Mass Transf 50:2272–2281
91. Ding Y, Chen H, He Y, Lapkin A, Yeganeh M, Siller L, Butenko YV (2007) Forced convective heat transfer of nanofluids. Adv Powder Technol 18:813–824
92. Willians W, Buongiorno J, Hu LW (2008) Experimental investigation of turbulent convective heat transfer and pressure loss of alumina/water and zirconia/water nanoparticle colloids (nanofluids) in horizontal tubes. J Heat Transf 130:042412
93. Hwang KS, Jang SP, Choi SUS (2009) Flow and convective heat transfer characteristics of water based Al_2O_3 nanofluids in fully developed laminar flow regime. Int J Heat Mass Transf 52:193–199
94. Jung J-Y, Oh H-S, Kwak H-Y (2009) Forced convective heat transfer of nanofluids in microchannels. Int J Heat Mass Transf 52:466–472
95. Rea U, McKrell T, Hu LW, Buongiorno J (2009) Laminar convective heat transfer and viscous pressure loss of alumina-water nanofluids. Int J Heat Mass Transf 52:2042–2048
96. Anoop KB, Sundararajan T, Das SK (2009) Effect of particle size on the convective heat transfer in nanofluid in the developing region. Int J Heat Mass Transf 52:2189–2195

97. Amrollahi A, Rashidi AM, Lotfi R, Meibodi EM, Kashefi K (2010) Convection heat transfer of functionalized MWNT in aqueous fluids in laminar and turbulent flow at the entrance region. Int Commun Heat Mass Transf 37:717–723
98. Liu ZH, Liao L (2010) Forced convective flow and heat transfer characteristics of aqueous drag-reducing fluid with carbon nanotubes added. Int J Therm Sci 49:2331–2338
99. Asirvatham LG, Raja B, Lal DM, Wongwises S (2011) Convective heat transfer of nanofluids with correlation. Particuology 9:626–631
100. Hojjat M, Etemad SG, Bagheri R, Thibault J (2011) Turbulent forced convection heat transfer of non-Newtonian nanofluids. Exp Therm Fluid Sci 35:1351–1356
101. Nasiri M, Etemad SG, Bagheri R (2011) Turbulent convective heat transfer of nanofluids through a square channel. Korean J Chem Eng 28:2230–2235
102. Suresh S, Chandrasekar M, Sekhar SC (2011) Experimental studies on heat transfer and friction factor characteristics of CuO/water nanofluid under turbulent flow in helically dimpled tube. Exp Therm Fluid Sci 35:542–549
103. Utomo AT, Poth H, Robbins TP, Pacek AW (2012) Experimental and theoretical studies on thermal conductivity, viscosity and heat transfer coefficient of titania and alumina nanofluids. Int J Heat Mass Transf 55:7772–7781
104. Heyhat MM, Kowsary F, Rashidi AM, Momenpour MH, Amrollahi A (2013) Experimental investigation of laminar convective heat transfer and pressure drop of water-based Al_2O_3 nanofluids in fully developed flow regime. Exp Therm Fluid Sci 44:483–489
105. Peyghambarzadeh SM, Shapouri S, Aslanzadeh N, Rahimnejad M (2013) Thermal performance of different working fluids in a dual diameter circular heat pipe. Ain Shams Eng J 4:855–861
106. Sahin B, Gültekin GG, Manay E, Karagoz S (2013) Experimental investigation of heat transfer and pressure drop characteristics of Al_2O_3-water nanofluid. Exp Therm Fluid Sci 50:21–28
107. Azmi WH, Sharma KV, Sarma PK, Mamat R, Najafi G (2014) Heat transfer and friction factor of water based TiO_2 and SiO_2 nanofluids under turbulent flow in a tube. Int Commun Heat Mass Transf 59:30–38
108. Chougule SS, Sahu SK (2014) Thermal performance of automobile radiator using carbon nanotube-water nanofluid—experimental study. J Therm Sci Eng Appl 6:041009
109. Sun B, Lei W, Yang D (2015) Flow and convective heat transfer characteristics of Fe_2O_3-water nanofluids inside copper tubes. Int Commun Heat Mass Transf 64:21–28
110. Karimzadehkhouei M, Yalcin SE, Sendur K, Mengüç MP, Kosar A (2015) Pressure drop and heat transfer characteristics of nanofluids in horizontal microtubes under thermally developing flow conditions. Exp Therm Fluid Sci 67:37–47
111. Gómez AOC, Hoffmann ARK, Bandarra Filho EP (2015) Experimental evaluation of CNT nanofluids in single-phase flow. Int J Heat Mass Transf 86:277–287
112. Li Y, Fernández-Seara J, Du K, Pardiñas AA, Latas LL, Jiang W (2016) Experimental investigation on heat transfer and pressure drop of ZnO/ethylene glycol-water nanofluids in transition flow. Appl Therm Eng 93:537–548
113. Colla L, Fedele L, Manca O, Marinelli L, Nardini S (2016) Experimental and numerical investigation on forced convection in circular tubes with nanofluids. Heat Transf Eng 37:1201–1210
114. Selvam C, Irshad MEC, Lal DM, Harish S (2016) Convective heat transfer characteristics of water-ethylene glycol mixture with silver nanoparticles. Exp Therm Fluid Sci 77:188–196
115. Sundar LS, Otero-Irurueta G, Singh MK, Souza ACM (2016) Heat transfer and friction factor of multi-walled carbon nanotubes-Fe_3O_4 nanocomposite nanofluids flow in a tube with/without longitudinal strip inserts. Int J Heat Mass Transf 100:691–703
116. Zarringhalam M, Karimipour A, Toghraie D (2016) Experimental study of the effect of solid volume fraction and Reynolds number on heat transfer coefficient and pressure drop of CuO-Water nanofluid. Exp Therm Fluid Sci 76:342–351
117. Gómez AOC, Alegrias JGP, Bandarra Filho EP (2017) Experimental analysis of the thermal-hydraulic performance of water based silver and SWCNT nanofluids in single-phase flow. Appl Therm Eng 124:1176–1188
118. Moreira TA, Alvariño PF, Cabezas-Gómez L, Ribatski G (2017) Experimental and numerical study of slightly loaded water alumina nanofluids in the developing region of a 1.1 mm in diameter pipe and convective enhancement evaluation. Int J Heat Mass Transf 115:317–335
119. Heyhat MM, Kowsary F (2010) Effect of particle migration on flow and convective heat transfer of nanofluids through a circular pipe. J Heat Transf 132:062401
120. Buongiorno J (2006) Convective transport in nanofluids. J Heat Transf 128:240–250
121. Kwark SM, Kumar R, Moreno G, Yoo J, You SM (2010) Pool boiling characteristics of low concentration nanofluids. Int J Heat Mass Transf 53:972–981
122. Vafaei S, Borca-Tasciuc T (2014) Role of nanoparticles on nanofluid boiling phenomenon: nanoparticle deposition. Chem Eng Res Des 92:842–856
123. White SB, Shih AJ, Pipe KP (2010) Effects of nanoparticle layering on nanofluid and base fluid pool boiling heat transfer from a horizontal surface under atmospheric pressure. J Appl Phys 107:1143021
124. Vafei S, Wen D (2010) Critical Heat Flux (CHF) of subcooled flow boiling of alumina nanofluids in a horizontal microchannel. J Heat Transf 132(10):102404
125. Souza RR, Passos JC, Cardoso EM (2014) Influence of nanoparticle size and gap size on nucleate boiling using HFE7100. Exp Therm Fluid Sci 59:195–201
126. Kim SJ, McKrell T, Buongiorno J, Hu LW (2009) Experimental study of flow critical heat flux in alumina-water, zinc-oxide-water, and diamond-water nanofluids. J Heat Transf 131:0432041
127. Forrest E, Williamson E, Buongiorno J, Hu LW, Rubner M, Cohen R (2010) Augmentation of nucleate boiling heat transfer and critical heat flux using nanoparticle thin-film coatings. Int J Heat Mass Transf 53:58–67
128. Santos Filho E, Nascimento FJ, Moreira DC, Ribatski G (2018) Dynamic wettability evaluation of nanoparticles-coated surfaces. Exp Therm Fluid Sci 92:231–242
129. Das SK, Putra N, Roetzel W (2003) Pool boiling of nano-fluids on horizontal narrow tubes. Int J Multiph Flow 29:1237–1247
130. Vassallo P, Kumar R, D'Amico S (2004) Pool boiling heat transfer experiments in silica-water nano-fluids. Int J Heat Mass Transf 47:407–411
131. Wen D, Ding Y (2005) Experimental investigation into the pool boiling heat transfer of aqueous based γ-alumina nanofluids. J Nanopart Res 7:265–274
132. Bang IC, Chang SH (2005) Boiling heat transfer performance and phenomena of Al_2O_3-water nano-fluids from a plain surface in a pool. Int J Heat Mass Transf 48:2407–4116
133. Park KJ, Jung D (2007) Enhancement of nucleate boiling heat transfer using carbon nanotubes. Int J Heat Mass Transf 50:4499–4502
134. Narayan GP, Anoop KB, Das SK (2007) Mechanism of enhancement/deterioration of boiling heat transfer using stable nanoparticle suspensions over vertical tubes. J Appl Phys 102:074317

135. Liu Z, Xiong J, Bao R (2007) Boiling heat transfer characteristics of nanofluids in a flat heat pipe evaporator with micro-grooved heating surface. Int J Multiph Flow 33:1284–1295
136. Kim SJ, Bang IC, Buongiorno J, Hu LW (2007) Surface wettability during pool boiling of nanofluids and its effects on critical heat flux. Int J Heat Mass Transf 50:4105–4116
137. Kim H, Buongiorno J, Hu LW, McKrell T, Dewitt G (2008) Experimental study on quenching of a small metal sphere in nanofluids. In: ASME International mechanical engineering congress and exposition, Boston, USA
138. Trisaksri V, Wongwises S (2009) Nucleate pool boiling heat transfer of TiO2-R141b nanofluids. Int J Heat Mass Transf 52:1582–1588
139. Park KJ, Jung D, Shin SE (2009) Nucleate heat transfer in aqueous solutions with carbon nanotubes up to critical heat fluxes. Int J Multiph Flow 35:525–532
140. Kedzierski MA, Gong M (2009) Effect of CuO nanolubricant on R134a pool boiling heat transfer. Int J Refrig 32:791–799
141. Suriyawong A, Wongwises S (2010) Nucleate pool boiling heat transfer characteristics of TiO_2-water nanofluids at very low concentrations. Exp Therm Fluid Sci 34:992–999
142. Kathiravan R, Kumar R, Gupta A, Chandra R (2010) Preparation and pool boiling characteristics of copper nanofluids over a flat plate heater. Int J Heat Mass Transf 53:1673–1681
143. Okawa T, Kamiya T (2010) Experimental studies on pool boiling characteristics of titanium dioxide water nanofluids. In: 18th International conference on nuclear engineering, Xi'an, China
144. Peng H, Ding G, Hu H, Jiang Y (2010) Influence of carbon nanotubes on nucleate pool boiling heat transfer characteristics of refrigerant-oil mixture. Int J Therm Sci 49:2428–2438
145. Liu ZH, Yang XF, Xiong JG (2010) Boiling characteristics of carbon nanotube suspensions under sub-atmospheric pressures. Int J Therm Sci 49:1156–1164
146. Kedzierski MA (2011) Effect of Al_2O_3 nanolubricant on R134a pool boiling heat transfer. Int J Refrig 34:498–508
147. Heris SZ (2011) Experimental investigation of pool boiling characteristics of low-concentrated CuO/ethylene glycol-water nanofluids. Int Commun Heat Mass Transf 38:1470–1473
148. Cieslinski JT, Kaczmarczyk TZ (2011) Pool boiling of water-Al_2O_3 and water-Cu nanofluids on horizontal smooth tubes. Nanoscale Res Lett 6:220–228
149. Huang CK, Lee CW, Wang KC (2011) Boiling enhancement by TiO_2 nanoparticle deposition. Int J Heat Mass Transf 54:4895–4903
150. Kathiravan R, Kumar R, Gupta A, Chandra R, Jain PK (2011) Pool boiling characteristics of multiwalled carbon nanotube (CNT) based nanofluids over a flat plate heater. Int J Heat Mass Transf 54:1289–1296
151. Yang XF, Liu ZH (2011) Pool boiling heat transfer of functionalized nanofluid under sub-atmospheric pressures. Int J Therm Sci 50:2402–2412
152. Ahmed O, Hamed MS (2012) Experimental investigation of the effect of particle deposition on pool boiling of nanofluids. Int J Heat Mass Transf 55:3423–3436
153. Wen D (2012) Influence of nanoparticles on boiling heat transfer. Appl Therm Eng 41:2–9
154. Kathiravan R, Kumar R, Gupta A, Chandra R (2012) Preparation and pool boiling characteristics of silver nanofluids over a flat plate heater. Heat Transf Eng 32:69–78
155. Kole M, Dey TK (2012) Investigations on the pool boiling heat transfer and critical heat flux of ZnO-ethylene glycol nanofluids. Appl Therm Eng 37:112–119
156. Duangthongsuk W, Yiamsawasd T, Selim Dalkilic A (2013) Pool-boiling heat transfer characteristics of Al_2O_3-water nanofluids on a horizontal cylindrical heating surface. Curr Nanosci 9:56–60
157. Shahmoradi Z, Etesami N, Esfahany MN (2013) Pool boiling characteristics of nanofluid on flat plate based on heater surface analysis. Int Commun Heat Mass Transf 47:113–120
158. Shoghl SN, Bahrami M (2013) Experimental investigation on pool boiling heat transfer of ZnO, and CuO water-based nanofluids and effect of surfactant on heat transfer coefficient. Int Commun Heat Mass Transf 45:122–129
159. Raveshi MR, Keshavarz A, Mojarrad MS, Amiri S (2013) Experimental investigation of pool boiling heat transfer enhancement of alumina-water-ethylene glycol nanofluids. Exp Therm Fluid Sci 44:805–814
160. Mohamadifard K, Heris SZ, Honarmand M (2014) Experimental investigation of pool boiling performance of alumina/ethylene-glycol/water (60/40) nanofluids. J Thermophys Heat Transf 28:724–734
161. Naphon P, Thongjing C (2014) Pool boiling heat transfer characteristics of refrigerant-nanoparticle mixtures. Int Commun Heat Mass Transf 52:84–89
162. Cieslinski JT, Krygier KA (2014) Augmentation of the critical heat flux in water-Al_2O_3, water-TiO_2 and water-Cu nanofluids. In: 10th International conference on heat transfer, fluid mechanics and thermodynamics, Orlando, USA
163. Kedzierski MA (2015) Effect of concentration on R134a/Al_2O_3 nanolubricant mixture on a reentrant cavity surface. Int J Refrig 49:36–48
164. Cieslinski JT, Kaczmarczyk TZ (2015) Pool boiling of water-Al_2O_3 and water-Cu nanofluids outside porous coated tubes. Heat Transf Eng 36:553–563
165. Sarafraz MM, Hormozi F (2015) Pool boiling heat transfer to dilute copper oxide aqueous nanofluids. Int J Therm Sci 90:224–237
166. Hu Y, Li H, He Y, Wang L (2016) Role of nanoparticle on boiling heat transfer performance of ethylene glycol aqueous solution based graphene nanosheets nanofluid. Int J Heat Mass Transf 96:565–572
167. Sarafraz MM, Hormozi F (2016) Experimental investigation on the pool boiling heat transfer to aqueous multi-walled carbon nanotube nanofluids on the micro-finned surfaces. Int J Therm Sci 100:255–266
168. Sarafraz MM, Hormozi F, Peyghambarzadeh SM (2016) Pool boiling heat transfer to dilute alumina nano-fluids on the plain and concentric circular micro-structures (CCM) surfaces. Exp Therm Fluid Sci 72:125–139
169. Ciloglu D (2017) An experimental investigation of nucleate pool boiling heat transfer of nanofluids from a hemispherical surface. Heat Transf Eng 38:919–930
170. Manetti LL, Stephen MT, Beck PA, Cardoso EM (2017) Evaluation of the heat transfer enhancement during pool boiling using low concentrations of Al_2O_3-water based nanofluid. Exp Therm Fluid Sci 87:191–200
171. Das SK, Narayan GP, Baby AK (2008) Survey on nucleate pool boiling of nanofluids: the effect of particle size relative to roughness. J Nanopart Res 10(7):1099–1108
172. Kiyomura IS, Manetti LL, Cunha AP, Ribatski G, Cardoso EM (2016) Analysis of the effects of nanoparticles deposition on characteristics of the heating surface and on pool boiling of water. Int J Heat Mass Transf 106:666–674
173. Kim SJ, Bang IC, Buongiorno J, Hu LW (2006) Effects of nanoparticle deposition on surface wettability influencing boiling heat transfer in nanofluids. Appl Phys Lett 89:153107
174. Bartelt K, Park Y, Liu L, Jacobi A (2008) Flow-boiling of R134a/POE/CuO nanofluids in a horizontal tube. In: International refrigeration and air conditioning conference, Purdue, USA

175. Peng H, Ding G, Jiang W, Hu H, Gao Y (2009) Heat transfer characteristics of refrigerant-based nanofluid flow boiling inside a horizontal smooth tube. Int J Refrig 32:1259–1270
176. Henderson K, Park YG, Liu L, Jacobi AM (2010) Flow-boiling heat transfer of R-134a-based nanofluids in a horizontal tube. Int J Heat Mass Transf 53:944–951
177. Boudouh M, Gualous HL, De Labachelerie M (2010) Local convective boiling heat transfer and pressure droop of nanofluid in narrow rectangular channels. Appl Therm Eng 30:2619–2631
178. Abedini E, Behzadmehr A, Rajabnia H, Sarvari SMH, Mansouri SH (2012) Experimental investigation and comparison of subcooled flow boiling of TiO_2 nanofluid in a vertical and horizontal tube. J Mech Eng Sci 227:1742–1753
179. Xu L, Xu J (2012) Nanofluid stabilizes and enhances convective boiling heat transfer in a single microchannel. Int J Heat Mass Transf 55:5673–5686
180. Yang XF, Liu ZH (2012) Flow boiling heat transfer in the evaporator of a loop thermosyphon operating with CuO based aqueous nanofluid. Int J Heat Mass Transf 55:7375–7384
181. Mahbubul IM, Saidur R, Amalina MA (2013) Heat transfer and pressure drop characteristics of Al_2O_3-R141b nanorefrigerant in horizontal smooth circular tube. Procedia Eng 56:323–329
182. Chehade AA, Gualous HL, Le Masson S, Fardoun F, Besqet A (2013) Boiling local heat transfer enhancement in minichannels using nanofluids. Nanoscale Res Lett 8:1–20
183. Rana KB, Rajvanshi AK, Agrawal GD (2013) A visualization study of flow boiling heat transfer with nanofluids. J Vis 16:133–143
184. Diao YH, Liu Y, Wang R, Zhao YH, Guo L, Tang X (2013) Effects of nanofluids and nanocoating on thermal performance of an evaporator with rectangular microchannels. Int J Heat Mass Transf 67:183–193
185. Akhavan-Behabadi MA, Nars M, Baqeri S (2014) Experimental investigation of flow heat transfer of R-600a/oil/CuO in a plain horizontal tube. Exp Therm Fluid Sci 58:105–111
186. Rana KB, Agrawal GD, Mathur J, Puli U (2014) Measurement of void fraction in flow boiling of ZnO-water nanofluids using image processing technique. Nucl Eng Des 270:217–226
187. Sun B, Yang D (2014) Flow boiling heat transfer characteristics of nano-refrigerants in a horizontal tube. Int J Refrig 38:206–214
188. Sarafraz MM, Hormozi F (2014) Convective boiling and particulate fouling of stabilized CuO-ethylene glycol nanofluids inside annular heat exchanger. Int Commun Heat Mass Transf 53:116–123
189. Sarafraz MM, Hormozi F (2014) Forced convective and nucleate flow boiling heat transfer to alumina nanofluids. Period Polytech 58:37–46
190. Duursma G, Sefiane K, Dehaene A, Harmand S, Wang Y (2015) Flow and heat transfer of single and two-phase boiling of nanofluids in microchannels. Heat Transf Eng 36:1252–1265
191. Yu L, Sur A, Liu D (2015) Flow boiling heat transfer and two-phase flow instability of nanofluids in a minichannel. J Heat Transf 137:051502
192. Setoodeh H, Keshavarz A, Ghasemian A, Nasouhi A (2015) Subcooled flow boiling of alumina/water nanofluid in a channel with a hot spot: an experimental study. Appl Therm Eng 90:384–394
193. Nikkhah V, Sarafraz MM, Hormozi F (2015) Application of spherical copper oxide (II) water nano-fluid as a potential coolant in a boiling annular heat exchanger. Chem Biochem Eng Q 29:405–415
194. Rajabnia H, Abedini E, Tahmasbi A, Behzadmehr A (2016) Experimental investigation of subcooled flow boiling of water/TiO_2 nanofluid in a horizontal tube. Therm Sci 20:99–108
195. Wang Y, Hu GH (2016) Experimental investigation on nanofluid flow boiling heat transfer in a vertical tube under different pressure conditions. Exp Therm Fluid Sci 77:116–123
196. Tazarv S, Saffar-Avval M, Khalvati F, Mirzaee E, Mansoori Z (2016) Experimental investigation of saturated flow boiling heat transfer to TiO_2/R141b nanorefrigerant. Exp Heat Transf 29:188–204
197. Sarafraz MM, Hormozi F (2016) Comparatively experimental study on the boiling thermal performance of metal oxide and multi-walled carbon nanotube nanofluids. Powder Technol 287:412–430
198. Karimzadehkhouei M, Sezen M, Sendur K, Mengüç MP, Kosar A (2017) Subcooled flow boiling heat transfer of γ-Al_2O_3/water nanofluids in horizontal microtubes and the effect of surface characteristics and nanoparticle deposition. Appl Therm Eng 127:536–546
199. Moreira TA, Nascimento FJ, Ribatski G (2017) An investigation of the effect of nanoparticle composition and dimension on the heat transfer coefficient during flow boiling of aqueous nanofluids in small diameter channels (1.1 mm). Exp Therm Fluid Sci 89:72–89
200. Sarafraz MM, Hormozi F (2014) Scale formation and subcooled flow boiling heat transfer of CuO-water nanofluid inside the vertical annulus. Exp Therm Fluid Sci 52:205–214
201. Kandlikar SG, Mizo VR, Cartwright MD (1997) Bubble nucleation and growth characteristics in subcooled flow boiling of water. In: ASME 32nd national heat transfer conference, Baltimore, USA
202. Liu Z, Winterton RHS (1991) A general correlation for saturation and subcooled flow boiling in tubes and annuli based on a nucleate pool boiling equation. Int J Heat Mass Transf 34:2759–2766
203. Cooper MG (1984) Saturation nucleate boiling: a simple correlation. In: 1st UK national conference on heat transfer, vol 2, pp 785–793